Seeding the Multi-dimensional Nonequilibrium Pulling for Hamiltonian Variation: Indirect QM/MM Free Energy Simulations

Zhaoxi Sun[1*] and Qiaole He[2]

[1]*Beijing National Laboratory for Molecular Sciences, College of Chemistry and Molecular Engineering, Institute of Theoretical and Computational Chemistry, Peking University, Beijing 100871, China*

[2]*State Key Laboratory of Bioreactor Engineering, East China University of Science and Technology, 200237 Shanghai, China*

*To whom correspondence should be addressed: z.sun@pku.edu.cn

Abstract

Combination of free energy simulations in the alchemical and configurational spaces provides a feasible route to access the thermodynamic profiles under a computationally demanding target Hamiltonian. Normally, due to the significant differences between the computational cost of ab initio quantum mechanics (QM) calculations and those of semi-empirical quantum mechanics (SQM) and molecular mechanics (MM), this indirect method could be used to obtain the QM thermodynamics by combining the SQM or MM results and the SQM-to-QM or MM-to-QM corrections. In our previous works, a multi-dimensional nonequilibrium pulling framework for Hamiltonian variations has been introduced based on bidirectional pulling and bidirectional reweighting. The method performs nonequilibrium free energy simulations in the configurational space to obtain the thermodynamic profile along the conformational change pathway under a selected computationally efficient Hamiltonian, and uses the nonequilibrium alchemical method to correct or perturb the thermodynamic profile to that under the target Hamiltonian. The BAR-based method is designed to achieve the best generality and transferability and thus leads to modest (~20 folds) speedup. In this work, we explore the possibility of further accelerating the nonequilibrium free energy simulation by employing unidirectional pulling and using the selection criterion to obtain the initial configurations used to initiate nonequilibrium trajectories following the idea of adaptive steered molecular dynamics (ASMD). A single initial condition is used to seed the whole multi-dimensional nonequilibrium free energy simulation and the sampling is performed fully in the nonequilibrium ensemble. The ASMD scheme estimates the free energy

difference with the unidirectional exponential average (EXP), but it does not follow exactly the requirements of the EXP estimator. Another deficiency of the seeding simulation is the inherently sequential or serial pulling due to the inter-segment dependency, which triggers some problems in the parallelizability of the simulation. Numerical tests are performed to grasp some insights and guidelines for using this selection-criterion-based ASMD scheme. The ASMD method is tested thoroughly on a dihedral flipping model system and encouraging numerical results are obtained. The presented selection-criterion-based multi-dimensional ASMD scheme follows the same perturbation framework of the BAR-based method, and thus could be used in various Hamiltonian-variation cases.

I. Introduction

All-atom molecular dynamics (MD) simulation is now a feasible tool to access the atomistic motions in complex systems. The statistically meaningful estimates of observables require extensive sampling of the phase space, and the sampling time depends on the intrinsic properties of the system, the description or Hamiltonian, and the sampling strategy. Probability distributions are often satisfactorily transformed to the free energy profiles or landscapes. The differences between the free energies of different states depict their relative stabilities.

Enhanced sampling simulations provide a computationally feasible route to obtain converged thermodynamics in complex systems.[1-4] They sample the system on modified energy landscapes to enhance the sampling efficiency and explore the phase space effectively.[3, 5-11] There are various types of enhanced sampling techniques. For instance, the traditional umbrella sampling[3, 12-14] adds a series of harmonic biasing potentials along the configurational collective variable (CV) to enhance the sampling efficiency in specific regions of phase space. The replica exchange method[15-20] designs a series of systems similar to the interested one but with higher flexibility in some degrees of freedom and attempts to exchange configurations in different equilibrium ensembles to enhance the barrier crossing and conformational search. The nonequilibrium steered MD (SMD) method shares similar features of the equilibrium umbrella sampling but adds time-independent biasing potential to drive the system from one state to another. The SMD approach is less frequently used, but is observed to be promising in various case studies.[8, 21-32] As the energy landscape is modified, proper post-processing methods are required to recover the statistics in the original unperturbed ensemble. Theoretically rigorous reweighting estimators in free energy simulations could be obtained based on free energy perturbation (FEP).[33] The estimator itself has many problems. For instance, the sample-size hysteresis problem[5-7] introduces significant biases into the finite-sample estimates, and the statistical error is heavily underestimated.[34, 35] These statistical problems could be avoided to some extent by combining the perturbations from multiple directions. In the two-state case, the statistically optimal estimator named Bennett Acceptance Ratio (BAR)[36, 37] uses the Fermi weighting function to process the data points, while in the multi-state situation the generalization of BAR named MBAR[38, 39] is of the highest statistical efficiency. The results obtained from perturbation-based reweighting estimators rely on the magnitude of phase space overlap between different states, and those of the neighboring states are often higher than the non-neighboring cases. As a result, the BAR estimates are often identical to the MBAR ones. The nonequilibrium generalization of the FEP derivatives replaces the energy difference with the nonequilibrium work (NEW) accumulated during nonequilibrium SMD simulations, and shares the same statistical problems

as the equilibrium perturbation schemes. The Jarzynski's Identity (JI)[40] corresponds to the exponential average (EXP) or FEP estimator, and the Crooks' Equation (CE)[41] is the nonequilibrium scenario of BAR. The equilibrium and nonequilibrium perturbation-based schemes are observed to achieve similar efficiency and accuracy in the construction of the potential of mean force (PMF) in various cases.[5-9, 21, 35, 42-48]

Complex processes often involve the rearrangements of multiple regions of the system, and it is difficult to find one or several proper CVs to describe these motions. Defining an optimal set of CVs requires a deep understanding of the dynamics of the system under investigation, which is very hard even for experienced researchers. For instance, the binding/unbinding event of protein-ligand complexes may involve significant conformational changes of the protein, which is hard to be captured with several CVs. The binding pathway may involve multiple ligand-residue interactions, some of which may be necessary to be included in the definition of the CV set. Considering the complexity of these problems, some alternative ways to obtain the variation of thermodynamics of the process could be preferred. The alchemical method only considers the differences between thermodynamics at physical end states. It avoids the direct simulation along the physical transformation pathway by defining an artificial alchemical order parameter.[47, 49-56] The free energy profile along this non-physical pathway is constructed and the overall free energy difference is obtained.[48, 57-61] As the alchemical method relies on the construction of a thermodynamic cycle to determine the relative free energy of different states,[48, 52, 55, 62-66] it could be viewed as an indirect regime to obtain the free energy difference. The alchemical method could also be used to perturb the description of the system.[67-77] For instance, the ab initio quantum mechanics (QM) results could be obtained by employing the alchemical method to perturb the semi-empirical QM (SQM) results.[34] The SQM results could also be obtained in a similar way by perturbing the thermodynamics obtained under some molecular mechanics (MM) force fields.[78] Due to the significant differences between the computational costs of different Hamiltonians, performing such perturbation could render some speedups compared with direct simulations under the computationally demanding Hamiltonians. In the case that the energetics under different Hamiltonians show significant differences, the staging technique should be used to improve the convergence behavior. However, equilibrium sampling in the intermediate states is computationally demanding, which actually degrades the efficiency of the indirect method. The situation is further aggravated when the configurational sampling in the intermediate state is difficult to converge.[48, 63, 79, 80] In this case, the nonequilibrium approach could be useful, as the intermediate-state sampling is avoided to some extent.

The combination of the enhanced sampling simulations in the configurational and alchemical spaces provides the multi-dimensional picture of the thermodynamic landscapes.[34, 76, 78, 81-92] The PMF along the

configurational CV at one alchemical state depicts the variations of thermodynamics in the process under that alchemical description/Hamiltonian, while the PMF along the alchemical CV at one configurational state shows the variations of some observables under different alchemical Hamiltonians or descriptions. Our previous works have provided a multi-dimensional nonequilibrium pulling framework for Hamiltonian variations, which features the stratification strategy, bidirectional pulling and bidirectional reweighting.[34, 78, 93] The BAR-based scheme obtains the thermodynamics along the configurational CV under some computationally efficient Hamiltonians such as SQM Hamiltonians, and perturbs the results to some ab initio levels with the alchemical method. Bidirectional pulling is used along both of these two perturbation pathways. However, as has been pointed out in the discussions of the previous works, the convergence of the simulation could be easily achieved in some cases,[34, 78, 93] and unidirectional pulling could be sufficient. Therefore, we explore the possibility of unidirectional pulling in the current work. A computationally efficient unidirectional pulling scheme in the SMD regime is the adaptive steered MD (ASMD) method, which relies on the stratification strategy and uses some selection criteria to obtain the initial configuration for the next nonequilibrium pulling segment from the configurations of the previous pulling segment. In this way, the initial configurational sampling in the SMD simulations is avoided and the efficiency is consequently improved. As only one or several configurations are used to spawn the whole nonequilibrium pulling simulations, the method could be considered as a seeding MD method. In the following parts, we would construct the multi-dimensional pulling framework in the ASMD regime and provide extensive tests on the perturbation parameters, aiming at providing some guidelines for using the method.

II. Methodology

The theoretical framework in the current work focuses on the variation of Hamiltonians or descriptions of the system. Each Hamiltonian defines a unique microscopic state of the simulated system, and we use the Hamiltonian H to describe the status of the system. The differences between the Hamiltonians could be, for instance, the details of the multi-scale treatment (e.g., the QM theory, the basis set, and the QM region). The microstate (k_1, k_2) is described with the state-specified Hamiltonian H_{k_1,k_2}, the two dimensions of which describe the conformational change and the description/model change, respectively. Consider the case that the thermodynamics under a target Hamiltonian $(..., K_2)$ is pursued. We explore the configurational space with $k_2 = 1$, and then perturb the results to another Hamiltonian $k_2 = K_2$. An illustration of the thermodynamic cycle is depicted in Fig. 1a. Unidirectional pulling and unidirectional reweighting are

performed in all perturbation parts, and only transformations drawn with solid arrows are performed. The reason that the thermodynamics along the configurational CV under the target Hamiltonian $H_{\ldots,k_2}$ could be efficiently obtained by the indirect method is that the conformational sampling could be much more time-consuming than the alchemical transformation. Rearrangements of many atoms or groups are involved in the process of interest.

During each nonequilibrium transformation in the configurational space, the time-dependent harmonic potential V given below is used to drive the system from one state to another,[94]

$$V(\mathbf{q}) = \frac{k}{2}\left(\xi(\mathbf{q}) - \xi_0(t)\right)^2 \quad (1).$$

Here, k is the force constant, $\mathbf{q}$ is the coordinate vector, $\xi_0(t)$ denotes the time-dependent protocol for CV variation defining the configurational transformation, and ξ refers to the current value of the CV. A large force constant could be used to suppress the fluctuations of the CV and keep the value of the CV very close to the predefined driving protocol, namely achieving the stiff spring limit.[21, 47, 78, 95-99] A small time step should be used to avoid unstable dynamics and the resulting perturbations of the distributions.[30-32, 34] The change of the alchemical order parameter follows exactly the predefined protocol.

Although the whole process could be simulated in one long pulling simulation, the dissipation is large and the waiting time before useful feedback is long. Therefore, to achieve a better numerical behavior and obtain faster user feedback, the whole pulling excursion could be divided into a series of shorter segments. As each of them could be finished in a much shorter simulation time and could be simulated independently, the parallelizability is improved and the output could be accessed much faster. Such pleasingly parallel computation also avoids the slowdown triggered by communications overhead, thus maximizing the performance. As the sampling in the configurational space is harder than that in the alchemical space, we only stratify the configurational sampling into K conformational states and $K-1$ segments. Note that for periodic configurational CV, the number of the conformational states is the same as that of the segments. As the convergence of the nonequilibrium pulling simulations depends heavily on the phase space overlap between different states and the magnitude of the perturbations during the nonequilibrium pulling process, the pulling simulations are only performed between neighboring states.

In our previous BAR-based pulling framework, we aim at achieving the best generality and transferability. Thus, the bidirectional statistically optimal estimator of BAR is employed. It achieves faster convergence compared with unidirectional EXP, and the upper bound of the statistical error is larger for BAR than EXP.[34, 35] However, the BAR-based scheme involves the pulling process from the target

Hamiltonian $H_{\ldots,K_2}$ to the selected Hamiltonian for configurational sampling $H_{\ldots,1}$, which might slightly increase the computational costs. Acceleration could be achieved by only performing unidirectional pulling from $H_{\ldots,1}$ to $H_{\ldots,K_2}$, as depicted in Fig. 1a. In this case, the EXP or JI estimator estimates the free energy difference by exponentially averaging the microscopic nonequilibrium works accumulated during nonequilibrium pulling simulations initiated from the *i*th state to the *j*th state,[40, 100] namely

$$\Delta A_{ij} = -\ln\left\langle e^{-W_{ij}}\right\rangle_i \tag{2}.$$

Here, ΔA denotes the dimensionless free energy difference, W_{ij} represents the dimensionless work accumulated during the nonequilibrium pulling initiated from state i and ended in state j, and $\langle\ldots\rangle_i$ represents the canonical average over nonequilibrium realizations initiated from state i. As the nonequilibrium transformations are performed between neighboring states, we have $j = i+1$ here. The estimator is valid for any pulling speeds, and such calculation is historically called the fast growth simulation. An alternative estimator applicable for extremely slow pulling speeds (i.e., reversible pulling) is the slow growth method.[101-103] In this case, the ordinary average of the microscopic nonequilibrium works is used to estimate the free energy difference, namely

$$\Delta A_{ij} = W_a = \left\langle W_{ij}\right\rangle_i \tag{3}.$$

The slow growth method is a variant of the equilibrium integration method thermodynamic integration.[101] The equation is valid for reversible pulling. However, practical simulations are all of finite lengths. Thus, the estimates are intrinsically biased.

Although the fast growth method is theoretically rigorous, as it is based on exponential averaging, it suffers from the same numerical problems of EXP, e.g., the sample size hysteresis and the underestimation of the statistical error. Cumulant expansion provides a way to better the numerical estimates from finite-length simulations. The expanded components are on the exponent and the free energy difference could be expressed as a linear combination of the cumulants.[104-106] The distribution of the nonequilibrium works in near-equilibrium pulling is close to Gaussian according to the central limit theory. For normally distributed data, only the first two terms in cumulant expansion survive, as higher-order cumulants are all zeros. Therefore, the Gaussian approximated EXP estimate GEXP could be expressed as

$$\Delta A_{ij} = \mu_{W_{ij}} - \frac{\sigma^2_{W_{ij}}}{2} \tag{4}.$$

Here, the mean of the works is μ, and σ is the standard deviation of the nonequilibrium works. The 1st

term is exactly the same as the slow growth estimate, and the 2nd term is an estimate of the dissipation of the pulling process, which corrects the bias of the slow growth result.

The statistical errors of the above three estimators could be obtained with the normal error propagation procedure. Note that for the EXP estimator, there is an upper bound for the analytical statistical error, which is found to be the thermal energy k_BT in our previous work.[35] The other two estimators of W_a and GEXP do not have this behavior.

The inputs of the above estimators and the corresponding statistical errors should be statistically independent. Thus, to initiate nonequilibrium pulling trajectories, equilibrium sampling in the initial state is required. The fluctuation of some observables could be used to define uncorrelated configurations. For instance, the autocorrelation of the reaction coordinate used to describe the conformational change was used to define uncorrelated initial configurations in dihedral flipping in peptides and nucleotide systems.[8, 9, 21, 47] Another example is the derivative of the alchemical Hamiltonian, which has been widely used in many alchemical free energy calculations.[60, 62, 65, 66, 107, 108] To obtain uncorrelated configurations, the autocorrelation time of the selected observable in each state τ_i is calculated and the whole dataset is subsampled by the statistical inefficiency $\phi_i = 1 + 2\tau_i$. The statistical inefficiency $\phi_{\mathrm{eq},i}$ is an estimate of the computational cost of each independent sample from equilibrium simulations, and the length of pulling simulations $\phi_{\mathrm{NEW},i}$ should be added to define the sampling time required for an independent sample in nonequilibrium pulling simulations, namely

$$\phi_i = \phi_{\mathrm{NEW},i} + \phi_{\mathrm{eq},i} \quad (5).$$

The pulling time $\phi_{\mathrm{NEW},i}$ for unidirectional pulling is the same as the pulling time in each segment, while that for bidirectional pulling should be multiplied by a factor of 2.

By using the above estimators to determine the free energy difference between all neighboring states, the variation of the free energy in the whole process could be obtained, namely

$$\Delta A_{1k} = \sum_{i=1}^{k-1} \Delta A_{i,i+1} \quad (6).$$

A reference state is often selected in the representation of the relative free energies. Here, the 1st state is selected and its free energy is set to zero. Then, the relative free energy of each state could be written as,

$$A_k = \Delta A_{1k} = \sum_{i=1}^{k-1} \Delta A_{i,i+1} \quad (7).$$

The procedure could be applied to both the alchemical and the configurational CVs. Combining the free energy profiles along these two CVs, the two-dimensional free energy surface depicting the variation of the thermodynamic profile in the configurational and alchemical spaces is obtained. The subscripts are altered in the multi-dimensional case. There are K_1 states and the state is numbered by k_1 for the configurational CV, while there are K_2 states and the state is numbered by k_2 for the alchemical CV. The reference state A_{11} has a free energy of zero, and the relative free energy of the state (k_1, k_2) is expressed as,

$$A_{k_1k_2} = \Delta A_{k_1 1,11} + \Delta A_{k_1k_2,k_1 1} = \sum_{i=1}^{k_1-1} \Delta A_{i,1,i+1,1} + \sum_{j=1}^{k_2-1} \Delta A_{k_1,j,k_1,j+1} \quad (8).$$

Here, $\Delta A_{k_1 1,11}$ is the free energy difference between the reference configurational state 1 and the configurational state k_1 at the 1st alchemical state, and $\Delta A_{k_1k_2,k_1 1}$ represents the perturbation term to change the alchemical state from 1 to k_2 at the k_1 th configurational state. The statistical fluctuation of the free energy estimates often makes the PMF noisy. Thus, the free energy profiles are smoothed with some curve fitting methods. Here, we use the Savitzky-Golay filter to increase the signal-to-noise ratio.

The above unidirectional perturbation framework presented above is a simple alternative to our previous BAR-based scheme. The free energy estimates could be obtained by performing initial configurational sampling in each Hamiltonian state, pulling the system between neighboring states, and using the EXP, GEXP or W_a estimator to get the free energy difference. However, we expect to further accelerate the simulations by introducing the selection criterion for initial configurations. The idea of the selection criterion arises from the fact that the ensemble of nonequilibrium configurations should include equilibrium snapshots.[109-111] Therefore, the last configurations of the *i*-to-(*i*+1) pulling simulations could possibly include the equilibrium structure(s) in the (*i*+1)th state. For small perturbations (i.e., slow pulling speeds), the existence of such equilibrium configuration(s) is expected to be extremely possible. Therefore, the initial configuration for the next stage (i.e., the (*i*+1)-to-(*i*+2) segment) could be obtained by selecting some configurations from the last configurations of the *i*-to-(*i*+1) segment. Here, we employ the naïve Jarzynski's scheme, where the configuration with the work nearest to the EXP estimate is selected.[47, 109-113] The ASMD simulation with the JI criterion is used to construct the free energy profile along the configurational CV, and the obtained initial configuration in each stage is also used to initiate the alchemical transformation. In this way, the need for equilibrium sampling in each intermediate is totally eliminated, thus accelerating the staged SMD simulations.

Although the selection criterion is useful to speed up the simulation, it has some drawbacks. First, the whole nonequilibrium pulling simulations are initiated from a single configuration, which leads to some correlations of the trajectories. As a result, the nonequilibrium works do not follow the requirement of the free energy estimators. There could be some biases in the free energy estimates, and the estimate of the corresponding statistical uncertainty is not theoretically rigorous. Whether this initial-configuration-induced bias would be significant requires some numerical tests. Second, although the whole pulling process is divided into a series of shorter segments, as the simulation starts from one segment (e.g., the reference state), all later segments need to wait for the output of the previous segments. Such inter-segment dependency leads to the poor parallelizability of ASMD simulations. Parallelization is possible only for the trajectories in the current segment and the computation of intra- and inter-molecular interactions in each simulation. The former leads to N_{traj} independent jobs for each segment, which could be run in parallel delightfully. However, the later parallelization suffers from parallel slowdown, and its efficiency depends on the size of the system, the way of the distributed computation and so on. Although the two parallelization schemes could be used simultaneously, the efficiency of the parallel computing is not as good as the previous BAR-based scheme, where all segments are independent and there are $N_{\text{segments}} * N_{\text{traj}}$ pulling simulations that could be run in parallel pleasingly. The limited parallelizability of ASMD simulations slows down the results output, which is further aggravated by the poor statistical behavior of the EXP estimator. The unidirectional EXP estimator often requires longer pulling times and larger sample sizes than the bidirectional BAR. Thus, a much longer waiting time is needed before user feedback, which is not a satisfactory behavior for protocol tests. However, the situation could be bettered to some extent if there are a series of similar systems (e.g., mutants of the same protein-ligand complex) under investigation. These similar systems could be simulated with the same protocol independently.

Convergence check is indispensable in free energy simulations. It ensures the reproducibility and the reliability of the simulation outputs, and thus should be tested in the first place. In the normal cases, we often monitor the sample-size and pulling-speed dependence of various ensemble averages.[34, 47, 52, 55, 78, 108] As the free energy is the generating function for other thermodynamic properties, we often focus on the free energy difference and the corresponding statistical uncertainty.[35, 52, 55, 108] Convergence is achieved when the free energy profile does not change with larger sample sizes or slower pulling speeds. The convergence diagnostics in the current ASMD case is a bit different. As the ASMD simulations along the configurational CV uses a predefined number of trajectories N_{traj}, we need to rerun the simulations with different N_{traj}

and check whether the results are invariant of this value. As the alchemical transformation is initiated from the configurations obtained during the ASMD simulations along the configurational CV and is finished in a single stage, we only need to test whether the number of trajectories is sufficient to converge the alchemical perturbation. The test of the pulling speed in ASMD simulations follows the same procedure as the normal staged SMD simulations. The same simulation procedure is repeated with different pulling speeds, and the convergence is reached when the free energy profile does not change with slower pulling speeds.

III. Computational Details

The Hamiltonian perturbation framework could be used to change various details of the system. In the current numerical test, we focus on the change of the QM theory. We still use the dihedral flipping system formed by caps of biomolecules ACE-NME in vacuo as an example. The reaction coordinate used to describe the dihedral flipping is the backbone C-C-N-C dihedral. We explore the configurational space with some SQM Hamiltonians, and then perform alchemical transformations to obtain the results under another Hamiltonian, e.g., ab initio QM or still some SQM Hamiltonians. An illustration of the thermodynamic cycle for the indirect free energy simulation is presented in Fig. 1b. In our previous works, we have considered SQM Hamiltonians of Austin Model 1 (AM1),[114] the Parametrized Model number 6 (PM6)[115] and the Modified Neglect of Diatomic Overlap (MNDO)[116], and ab initio QM ones such as the Hartree-Fock method (HF),[117-119] the second-order perturbation theory (MP2),[120-123] the Becke 3-parameter Lee–Yang–Parr (B3LYP) functional,[124-126] and the ωB97X-D functional[127]. This time we consider another SQM Hamiltonian with good accuracy but is less frequently used. Recife Model 1 (RM1)[128] is an improved version of AM1. It provides better descriptions of various observables and thus is considered as a target SQM Hamiltonian in the current work. The HF method is still used as an ab initio target in this work. Therefore, in this work, we aim at obtaining the RM1 and HF results indirectly with the selection-criterion-based multi-dimensional nonequilibrium pulling simulations.

The nonequilibrium trajectories are simulated independently and a single core is distributed to each trajectory. This avoids the parallel slowdown that degrades the performance of the simulation. In Table S1, we present the single-core timing data. The costs of the SQM simulations are extremely similar, and the HF simulation is much more costly than the SQM ones.

As a single structure is used to spawn the whole ASMD pulling process, we test the influence of using different configurations as the initial seed. The ASMD pulling starts at the 0° state, which is used as the reference state with a free energy of zero. The system is constructed in vacuo and equilibrated for 50 ps

under the AMBER14SB[129] force field. Then, we shift to the SQM Hamiltonian and equilibrate the system for 50 ps. Finally, we perform the production run to extract independent configurations to investigate the influence of the initial seed, and extract 8 configurations every 90 ps to avoid any possible correlations between the initial seeds.

The whole dihedral flipping process from 0° to 360 ° is divided into 120 segments with 3 ° increments. The force constant of 2000 kcal/mol·rad^2 is used to achieve the stiff spring limit. As for the pulling speed and the sample size for each segment, some related statistics of ASMD simulations could be obtained from our previous works.[47] Our previous experience on the dihedral flipping case indicates that 20-sample and 40-sample estimates are identical in the configurational pulling. Thus, the sample size in each segment along the configurational CV is 20. The simulation outcome shows a higher sensitivity on the pulling speed. The pulling speed of 8 ps per 5º was used in our previous work, which corresponds to a pulling time of approximately 5 ps for the 3º segment used in this work. The previous work is performed under the MM Hamiltonian while in the current work we use some SQM Hamiltonians. As the fluctuations under different Hamiltonians are different, some tests should be performed on the pulling speed to ensure that our results are converged on this degree of freedom. 5 ps, 10 ps, and 15 ps are tested for the current 3º segment in the configurational space. The alchemical transformation uses the initial configurations obtained with the selection criterion in the ASMD simulations along the configurational CV. In the previous BAR-based case, bidirectional alchemical transformations finished in several time steps are sufficient to converge the results.[34] In the current EXP-based case, the statistical efficiency is a bit worse and thus we employ longer pulling times for the alchemical transformation. The relaxation time between successive perturbations is set to 1 time step and the transformation is finished in 10 or 100 time steps, corresponding to a change of 0.1 or 0.01 per time step for the alchemical order parameter.

In all MD simulations, the time step is set to 0.5 fs, and Langevin dynamics[130] with the collision frequency of 5 ps^{-1} are implemented for temperature regulation at 300 K. As the simulation is performed in vacuo, there is no cutoff applied in our simulations. Although the current simulation is performed in vacuo, the Hamiltonian variation framework could be straightforwardly applied in condensed-phase simulations, which has been performed in our previous works.[34, 78] We use the AMBER[131] suite for MD simulations and Gaussian 09[132] for ab initio QM calculations. All statistical analyses are obtained with homemade codes.

IV. Result and discussion

The pulling-speed and sample-size dependence of the estimates.

As discussed in the last part of the methodology section, the convergence diagnostics should be performed in the first place before analyzing detailed results. We choose the target RM1 Hamiltonian as an example. The pulling-speed dependence of the free energy profile in direct free energy simulations at the RM1 level is presented in Fig. 2a. The 10 ps/segment (i.e., 20000 steps) PMF is virtually identical to the 15 ps/segment results, and minor differences are observed for the 5 ps/segment result. Therefore, in the nonequilibrium pulling along the configurational CV, we use the pulling speed of 10 ps/segment. We then check the sample-size dependence of the indirect estimates obtained with the pulling time of 10 steps in the alchemical space. In Fig. 2b, the comparison between the indirect estimates obtained from the AM1 simulations with different sample sizes and different estimators for the AM1-to-RM1 perturbation from one initial seed and the direct RM1 PMF is presented. We can see that the 5-sample, 10-sample and 50-sample estimates obtained from the EXP, GEXP and W_a estimators are all identical, which indicates that the sample size is not a bottleneck for the convergence of the nonequilibrium free energy simulation. Namely, the estimates are numerically stable and could be converged easily. The difference between the indirect and direct estimates are small, but we expect to further minimize this deviation.

The agreement between the EXP, GEXP and W_a estimates does not necessarily indicate the convergence of the nonequilibrium pulling simulations. The configurational sampling in the equilibrium perturbation scheme is performed in the equilibrium ensemble, while that in the nonequilibrium pulling case required by JI or CE is performed in both the equilibrium ensemble and the nonequilibrium pulling. The ASMD scheme uses a single structure to seed a series of nonequilibrium simulations, from which the microscopic nonequilibrium works are extracted. As a result, these microscopic nonequilibrium works are not independent and thus do not fully satisfy the assumption of the JI estimator. The inter-trajectory correlation is significant when the nonequilibrium pulling simulation is very short. For instance, when the nonequilibrium pulling is finished in just one step, the nonequilibrium work reduces to the energy difference in the equilibrium perturbation scheme, and the nonequilibrium works from different pulling simulations are exactly the same. Significant systematic bias is introduced in this case. Further, the EXP, GEXP and W_a estimates are exactly the same, which provides no hints on the dissipation of the nonequilibrium trajectories. Therefore, to achieve a sufficient level of configurational sampling, the nonequilibrium trajectories should not be too short. The calculation of the statistical error also has this problem. As the analytical formula of the statistical uncertainty requires independent works as input, the statistical error could be underestimated in ASMD simulations. The initial-configuration-induced systematic bias is significant for the alchemical

transformation due to the short length of such pulling simulation, but is very small for the configurational part, as the long pulling time in the latter simulations enables sufficient sampling in the nonequilibrium ensemble.

Although the EXP, GEXP and W_a estimates are virtually identical, obvious differences could be observed for their statistical errors. We focus on the alchemical perturbation to the RM1 level and the results obtained with the pulling speed of 10 ps/segment in the configurational space and a pulling time of 10 steps in the alchemical space are presented in Fig. 3a. We can see that the statistical uncertainty of the EXP estimator is much smaller than the others for all of the three alchemical transformations to the RM1 level considered in the current work. The GEXP and W_a estimators have extremely similar statistical uncertainties, which is expected considering the agreement between the free energy estimates obtained from these two estimators. The first term of GEXP is the ordinary average of the microscopic works W_a, and the second term relates to the variance of the work distribution. When the GEXP and W_a estimates are virtually identical, the width of the work distribution is negligible, and the resulting statistical errors of these two estimators are extremely similar. Fig. 3b shows the dependence of the statistical uncertainty on the pulling speed in the configurational space for the AM1-to-RM1 transformation. Still, the EXP uncertainty is much smaller than the others. The statistical uncertainties obtained with the pulling speeds of 10 ps/segment and 15 ps/segment are extremely similar, which indicates that the pulling time in the configurational space is sufficiently long and the simulation outcome does not depend on this pulling speed.

Indirect vs direct.

After testing the pulling speed and the sample size in nonequilibrium free energy simulations, we then test the probably most influencing parameter, the initial seed. As discussed in the previous part, the initial configuration has a larger impact on the alchemical part due to the short transformation length of the nonequilibrium pulling, while in the configurational space the lack of sampling in the equilibrium ensemble (i.e., the initial configuration) is compensated with the sampling in the nonequilibrium ensemble during the long pulling time. To provide a clearer presentation of the initial-configuration-induced bias, we compare the indirect estimates obtained from different initial seeds with the direct RM1 result. The indirect estimates obtained from PM6, AM1 and MNDO are presented in Fig. S1 and S2. If not explicitly mentioned, the alchemical perturbation is finished in 10 steps in these cases.

For the PM6 Hamiltonian, longer pulling time in the configurational space does not necessarily result in better indirect estimates, as shown in Fig. S1a-b. The indirect estimates with the pulling speed of 10

ps/segment in the configurational space fluctuate around the direct RM1 result, as shown in Fig. S1a, c, d and e. This is expected as the sampling in the nonequilibrium ensemble is insufficient for the alchemical transformation. The situation could be bettered by performing longer pulling simulations in the alchemical space. The indirect result becomes closer to the direct RM1 estimate when the alchemical perturbation is finished in 100 steps.

Systematic investigations at the AM1 and MNDO levels could be more informative. The indirect estimates obtained from ASMD simulations initiated from one initial configuration with the pulling speed of 10 ps/segment in the configurational space and a pulling time of 10 steps in the alchemical space is presented in Fig. 4a, and the indirect estimates obtained from 8 initial seeds with the same pulling scheme are presented in Fig. S2a-h. We can see that the indirect estimates seem to fluctuate around the RM1 result. For some initial seeds, the accord between the indirect and direct estimates could be good, while for the others the agreement is not so satisfactory. The results obtained with slower pulling speeds in the configurational space are presented in Fig. S2i-k, from which we observe that longer pulling time in the configurational space does not help to improve the indirect estimates.

As has been discussed above, to better the indirect estimate, we need to perform more sampling either in the equilibrium ensemble or in the nonequilibrium one. If we want to distribute the sampling in the equilibrium ensemble, we need more uncorrelated configurations to initiate the nonequilibrium alchemical transformation and average over these simulations to obtain a more accurate and stable estimate, which could be achieved by either equilibrating the initial configurations obtained with the selection criterion from one ASMD trail or performing multiple ASMD simulations initiated from different seeds. The former scheme could be easily performed and the results are expected to be good, while the performance of the latter regime is not straightforward and thus our numerical test focuses on this scheme. The results averaged over 5 initial seeds are presented in Fig. 4b, from which we can see that the agreement between the indirect and direct estimates is improved. The mean absolute error (MAE) is calculated to provide some numerical metrics to assess the deviation of the indirect estimate from the direct result, which is presented in Table 1. We can see that the MAE for the initial-configuration-averaged estimate is much smaller than the individual estimates. Another way to improve the result is distributing the sampling in the nonequilibrium ensemble, namely lengthening the pulling time in the alchemical space. We employ a longer pulling time of 100 steps in the alchemical transformation with a change of 0.01 per time step for 5 of the initial seeds, and the results are presented in Fig. 4c and Fig. S3a-d. We can see that the indirect estimates are effectively improved by using a slower pulling speed along the alchemical CV. Again, we use a longer pulling time in the

configurational space in Fig. S3e-f, where we observe that the pulling speed in the configurational space has little impact on the simulation outcome. The indirect estimate could be improved by using both the slower-pulling-speed and initial-seed-averaging schemes, the result of which is shown in Fig. 4d. The MAEs of the 0.01 indirect estimates shown in Table 1 are smaller than the corresponding 0.1 components, and the seed-averaged result achieves an MAE of about 0.09 kcal/mol, which is technically speaking negligible in free energy calculations.

Hitherto, we have gained some insights into using the ASMD-based indirect nonequilibrium free energy simulation scheme. We then employ the scheme to obtain the HF result indirectly. We still use the same pulling speed in nonequilibrium pulling, i.e., 10 ps/segment in the configurational space and 10 or 100 steps in the alchemical transformation. The MAEs of 7 trails with a change of 0.1 per step in the alchemical transformation and that of one trail with a change of 0.01 per step are presented in Table S2. We can see that the HF result could be obtained with the ASMD-based indirect scheme with an MAE ~0.25 kcal/mol. The previous RM1-from-SQM simulations do not result in a speedup of the free energy simulation, but the current HF-from-SQM one does accelerate the simulation. Thus, we then calculate the speedup of the indirect scheme. When performing free energy simulations in the configurational space, it requires 24 ns to converge the free energy profile. The pulling time of 10 steps is used for the alchemical transformation. 5 samples are sufficient to converge the alchemical term for each initial seed and 5 repeats/seeds are averaged to obtain the final indirect result with very good convergence behavior. The need for equilibrium configurational sampling to obtain the initial configurations is eliminated and thus ϕ_{eq} is set to zero. The simulation time at the HF level is scaled by the simulation speeds in Table S1 to obtain the effective sampling time at the SQM level. The resulting speedup of the indirect scheme is about 1000-fold, as shown in Table 2. If we use the pulling time of 100 steps for the alchemical transformation, the resulting indirect estimate would be extremely accurate and the speedup would be about 200 folds. The computational speedup could also be compared with the statistics of the BAR-based scheme in our previous work,[34] which is presented in Table 3. As the BAR-based scheme achieves faster convergence than the ASMD regime in the configurational sampling,[47] the speedup of the ASMD-based indirect scheme is relatively modest compared with the ~1000-fold speedup shown in the previous table. However, the speedup of the indirect scheme is still two orders of magnitude.

In the BAR-based scheme, the computational cost of the direct SQM free energy simulation is negligible. The reasons for this phenomenon include the significant difference between the computational cost of the target ab initio QM Hamiltonian and that of the SQM Hamiltonian, the inclusion of the

computationally demanding equilibrium sampling at ab initio QM level to obtain initial configurations for nonequilibrium alchemical transformation, and the high statistical efficiency of the bidirectional estimator. As a result, the speedup of the indirect scheme could be approximated with the ratio of the sampling time in the direct QM free energy simulation to that in the SQM-to-QM perturbation, namely

$$\text{speedup} \approx \frac{n_{\text{direct QM}}\phi_{\text{direct QM}}}{n_{\text{SQM-to-QM correction}}\phi_{\text{SQM-to-QM correction}}} = \frac{\phi_{\text{NEW,direct QM}} + \phi_{\text{eq}}}{\phi_{\text{NEW,SQM-to-QM correction}} + \phi_{\text{eq}}} \quad (9).$$

Here, the equal-sample-size rule is used for the direct and the alchemical perturbation terms. However, in the current ASMD case, the equilibrium sampling for initial configurations is avoided, and the computational cost of the direct SQM free energy simulation is non-negligible. A key feature that is unchanged is that the main contribution of the computational cost of the indirect free energy simulation still comes from the SQM-to-QM transformation.

V. Conclusion

The combination of the alchemical and configurational free energy simulations provides a computationally feasible alternative to obtain the thermodynamics at ab initio QM levels. The free energy landscape obtained from enhanced sampling simulations under a computationally feasible Hamiltonian could be perturbed to that under another Hamiltonian with the alchemical method. In our previous works, we constructed a multi-dimensional nonequilibrium pulling framework for Hamiltonian variation based on bidirectional pulling and bidirectional reweighting. The BAR-based method is generally applicable and the acceleration of the indirect method is about an order of magnitude compared with the direct free energy simulations under some ab initio QM Hamiltonians. As bidirectional pulling could be costly in some cases, in the current work, we alter the bidirectional perturbation framework to a unidirectional one and use the exponential average, its Gaussian approximated form, and the ordinary average to estimate the free energy difference. The staged SMD simulation is further accelerated with the selection criterion for the initial configuration used to initiate nonequilibrium trajectories. This ASMD-based Hamiltonian variation framework is more than 100-fold faster than the direct free energy simulations under some ab initio QM Hamiltonian.

A worth noting behavior of the ASMD-based scheme is the distribution of the sampling. In the normal staged SMD pulling with JI or CE for free energy estimates, equilibrium sampling in each intermediate state is performed to obtain the initial configuration for kicking off the pulling simulations. The sampling is distributed in both the equilibrium ensemble and the nonequilibrium counterpart. However, as the

nonequilibrium trajectories are initiated from one initial configuration in ASMD simulations, some alternations of the simulation scheme are required. We can distribute some sampling times in the equilibrium ensemble by equilibrating the initial configuration obtained from the selection criterion, or performing ASMD simulations from different initial seeds to obtain more initial configurations. In this way, more independent initial configurations are obtained and nonequilibrium alchemical pulling simulations from these uncorrelated configurations could improve the convergence behavior of the indirect scheme. Alternatively, we can sample only in the nonequilibrium ensemble by pulling it slower in the alchemical space, which also improves the convergence behavior of the indirect scheme. The initial-seed-averaging and slower-pulling-speed schemes could be combined to achieve better numerical behaviors.

Although the JI-based ASMD scheme could be efficient for multi-dimensional nonequilibrium pulling, there are still some weaknesses. As the whole pulling simulation is initiated from one or several configurations, the nonequilibrium pulling in the configurational space is performed in a serial way. Specifically in the current dihedral flipping case, the simulation is initiated from the 0º state and the pulling is performed from this reference state to the other in a serial manner. The 3º-to-6º pulling simulations need to wait for the outcome of the 0º-to-3º simulations, and the 6º-to-9º pulling simulations need to wait for the outcome of the 3º-to-6º simulations. This inter-segment dependence limits the efficiency of parallelism and we can only parallelize the nonequilibrium trajectories of the current segment. Although the calculation of the energetics of each simulation could also be parallelized, the efficiency of this parallel computation is degraded compared with the delightfully parallel BAR-based scheme even for parallel-optimized dynamic engines (i.e., the so-called parallel slowdown due to communications overhead). A factor that further aggravates this parallel issue is the need for slower pulling speeds when using the exponential average. Compared with bidirectional reweighting, the lower statistical efficiency of EXP requires a longer pulling time to obtain converged estimates and thus the waiting time for each segment is lengthened. The overall outcome of these factors is a longer waiting time before user feedback, which is not a satisfactory property for protocol diagnosing. However, if the user already has some experiences on the convergence behavior of the system (e.g., after the protocol testing procedure), or if there are a series of systems with similar properties (e.g., a series of mutants of some protein-ligand complexes), the EXP-based ASMD scheme could save the computational costs significantly. Note that the tests of a series of different protocols could also be performed independently, and the parallelization in this case could also be useful. However, the user still needs to wait for the output of the longer/longest protocol with the higher/highest reliability before he/she is able to confirm whether the faster protocols are reliable.

Acknowledgement

This work was supported by the National Natural Science Foundation of China (Grant No. 21633001). Part of the simulation was performed on the high-performance computing platform of the Center for Life Science (Peking University). Dr. Zhaoxi Sun is supported by the PKU-Boya Postdoctoral Fellowship. We thank anonymous reviewers for valuable comments and critical reading.

Conflicts of interest

There are no conflicts of interest to declare.

Supporting information

The single-core timing information of SQM and ab initio QM simulations, MAEs of the indirect estimates at ab initio QM levels, comparison between the direct and indirect estimates at the RM1 level initiated from different seeds with different pulling speeds are provided in the supporting information.

References

1. Echeverria, I.; Amzel, L. M., Helix propensities calculations for amino acids in alanine based peptides using Jarzynski's equality. *Proteins: Structure, Function, and Bioinformatics* **2010**, 78, 1302-1310.

2. Lee, T. S.; Radak, B. K.; Huang, M.; Wong, K. Y.; York, D. M., Roadmaps through free energy landscapes calculated using the multi-dimensional vFEP approach. *J. Chem. Theory Comput.* **2014**, 10, 24-34.

3. Sun, Z.; Wang, X.; Zhang, J. Z. H., Protonation-dependent Base Flipping in The Catalytic Triad of A Small RNA. *Chemical Physics Letters* **2017**, 684, 239-244.

4. Moraca, F.; Amato, J.; Ortuso, F.; Artese, A.; Pagano, B.; Novellino, E.; Alcaro, S.; Parrinello, M.; Limongelli, V., Ligand binding to telomeric G-quadruplex DNA investigated by funnel-metadynamics simulations. *Proc. Natl. Acad. Sci. U.S.A.* **2017**, 114, E2136-E2145.

5. Wood, R. H.; Muhlbauer, W. C. F.; Thompson, P. T., Systematic errors in free energy perturbation calculations due to a finite sample of configuration space: sample-size hysteresis. *Journal of Physical Chemistry* **1991**, 95, 6670-6675.

6. Gore, J.; Ritort, F.; Bustamante, C., Bias and error in estimates of equilibrium free-energy differences from nonequilibrium measurements. *Proc. Natl. Acad. Sci. USA* **2003**, 100, 12564-12569.

7. Zuckerman, D. M.; Woolf, T. B., Theory of a systematic computational error in free energy differences. *Physical Review Letters* **2002**, 89, 180602.

8. Sun, Z.; Wang, X.; Zhang, J. Z. H.; He, Q., Sulfur-substitution-induced base flipping in the DNA duplex. *Phys. Chem. Chem. Phys.* **2019**, 21, 14923-14940.

9. Sun, Z.; Zhang, J. Z. H., Thermodynamic Insights of Base Flipping in TNA Duplex: Force Fields, Salt Concentrations, and Free-Energy Simulation Methods. *CCS Chemistry* **2020**, 2, 1026–1039.

10. Lemkul, J. A.; Savelyev, A.; MacKerell Jr, A. D., Induced Polarization Influences The Fundamental Forces in DNA Base Flipping. *J. Phys. Chem. Lett.* **2014**, 5, 2077-2083.

11. Sun, Z.; He, Q.; Li, X.; Zhu, Z., SAMPL6 host–guest binding affinities and binding poses from spherical-coordinates-biased simulations. *Journal of Computer-Aided Molecular Design* **2020**, 34, 589-600.

12. Mezei, M., Adaptive Umbrella Sampling: Self-consistent Determination of the Non-Boltzmann Bias. *J. Comput. Phys.* **1987**, 68, 237-248.

13. Hooft, R. W.; van Eijck, B. P.; Kroon, J., An Adaptive Umbrella Sampling Procedure in Conformational Analysis using Molecular Dynamics and Its Application to Glycol. *J. Chem. Phys.* **1992**, 97, 6690-6694.

14. Kästner, J., Umbrella sampling. *Wiley Interdisip. Rev. Comput. Mol. Sci.* **2011**, 1, 932-942.

15. Fukunishi, H.; Watanabe, O.; Takada, S., On the Hamiltonian replica exchange method for efficient sampling of biomolecular systems: Application to protein structure prediction. *J. Chem. Phys.* **2002**, 116, 9058-9067.

16. Itoh, S. G.; Damjanovic, A.; Brooks, B. R., pH replica-exchange method based on discrete protonation states. *Proteins* **2011**, 79, 3420-36.

17. Okur, A.; Wickstrom, L.; Layten, M.; Geney, R.; Song, K.; Hornak, V.; Simmerling, C., Improved Efficiency of Replica Exchange Simulations through Use of a Hybrid Explicit/Implicit Solvation Model. *J. Chem. Theory Comput.* **2006**, 2, 420.

18. Sabri, D. D.; Roitberg, A. E., Optimization of Umbrella Sampling Replica Exchange Molecular Dynamics by Replica Positioning. *J. Chem. Theory Comput.* **2013**, 9, 4692–4699.

19. Sugita, Y.; Okamoto, Y., Replica-exchange molecular dynamics method for protein folding. *Chemical physics letters* **1999**, 314, 141-151.

20. Sugita, Y.; Kitao, A.; Okamoto, Y., Multidimensional replica-exchange method for free-energy calculations. *J. Chem. Phys.* **2000**, 113, 6042-6051.

21. Wang, X.; Sun, Z., Determination of Base Flipping Free Energy Landscapes from Nonequilibrium Stratification. *J. Chem. Inf. Model.* **2019**, 59, 2980-2994.

22. Procacci, P., Accuracy, precision, and efficiency of nonequilibrium alchemical methods for computing free energies of solvation. I. Bidirectional approaches. *J. Chem. Phys.* **2019**, 151, 144113.

23. Chelli, R.; Procacci, P., A potential of mean force estimator based on nonequilibrium work exponential averages. *Phys. Chem. Chem. Phys.* **2009**, 11, 1152-1158.

24. Chelli, R.; Marsili, S.; Barducci, A.; Procacci, P., Recovering the Crooks equation for dynamical systems in the isothermal-isobaric ensemble: a strategy based on the equations of motion. *J. Chem. Phys.* **2007**, 126, 044502.
25. Procacci, P., Unbiased free energy estimates in fast nonequilibrium transformations using Gaussian mixtures. *J. Chem. Phys.* **2015**, 142, 2690-2693.
26. Nicolini, P.; Frezzato, D.; Chelli, R., Exploiting configurational freezing in nonequilibrium Monte Carlo simulations. *J. Chem. Theory Comput.* **2011**, 7, 582-593.
27. Chelli, R.; Marsili, S.; Barducci, A.; Procacci, P., Generalization of the Jarzynski and Crooks nonequilibrium work theorems in molecular dynamics simulations. *Phys. Rev. E* **2007**, 75, 050101.
28. Nerattini, F.; Chelli, R.; Procacci, P., II. Dissociation free energies in drug–receptor systems via nonequilibrium alchemical simulations: application to the FK506-related immunophilin ligands. *Phys. Chem. Chem. Phys.* **2016**, 18, 15005-15018.
29. Chelli, R.; Gellini, C.; Pietraperzia, G.; Giovannelli, E.; Cardini, G., Path-breaking schemes for nonequilibrium free energy calculations. *J. Chem. Phys.* **2013**, 138, 214109.
30. Fass, J.; Sivak, D. A.; Crooks, G. E.; Beauchamp, K. A.; Leimkuhler, B.; Chodera, J. D., Quantifying configuration-sampling error in Langevin simulations of complex molecular systems. *Entropy* **2018**, 20, 318.
31. Sivak, D. A.; Chodera, J. D.; Crooks, G. E., Time Step Rescaling Recovers Continuous-Time Dynamical Properties for Discrete-Time Langevin Integration of Nonequilibrium Systems. *J. Phys. Chem. B* **2014**, 118, 6466-6474.
32. Sivak, D. A.; Chodera, J. D.; Crooks, G. E., Using Nonequilibrium Fluctuation Theorems to Understand and Correct Errors in Equilibrium and Nonequilibrium Simulations of Discrete Langevin Dynamics. *Phys. Rev. X* **2013**, 3, 011007.
33. Zwanzig, R. W., High Temperature Equation of State by A Perturbation Method. *J. Chem. Phys.* **1954**, 22, 1420-1426.
34. Sun, Z., BAR-based multi-dimensional nonequilibrium pulling for indirect construction of QM/MM free energy landscapes: from semi-empirical to ab initio. *Phys. Chem. Chem. Phys.* **2019**, 21, 21942-21959
35. Wang, X.; Sun, Z., A Theoretical Interpretation of Variance-based Convergence Citeria in Perturbation-based Theories. *arXiv preprint arXiv:1803.03123* **2018**.
36. Shirts, M. R.; Bair, E.; Hooker, G.; Pande, V. S., Equilibrium Free Energies from Nonequilibrium Measurements using Maximum-likelihood Methods. *Physical review letters* **2003**, 91, 140601.
37. Bennett, C. H., Efficient Estimation of Free Energy Differences from Monte Carlo data. *J. Comput. Phys.* **1976**, 22, 245-268.
38. Tan, Z., On a Likelihood Approach for Monte Carlo Integration. *J. Am. Stat. Assoc.* **2004**, 99, 1027-1036.
39. Shirts, M. R.; Chodera, J. D., Statistically optimal analysis of samples from multiple equilibrium states. *J. Chem. Phys.* **2008**, 129, 124105.
40. Jarzynski, C., A Nonequilibrium Equality for Free Energy Differences. *Physical Review Letters* **1997**, 78, 2690-2693.
41. Mallick, K.; Moshe, M.; Orland, H., Supersymmetry and Nonequilibrium Work Relations. *arXiv preprint arXiv:0711.2059* **2008**.
42. Ballard, A. J.; Jarzynski, C., Replica exchange with nonequilibrium switches: enhancing equilibrium sampling by increasing replica overlap. *J. Chem. Phys.* **2012**, 136, 194101.
43. Vaikuntanathan, S.; Jarzynski, C., Escorted free energy simulations: improving convergence by reducing dissipation. *Physical Review Letters* **2008**, 100, 190601.
44. Dickson, A.; Dinner, A. R., Enhanced Sampling of Nonequilibrium Steady States. *Annual Review of Physical Chemistry* **2010**, 61, 441-459.
45. Hudson, P. S.; Woodcock, H. L.; Boresch, S., Use of Nonequilibrium Work Methods to Compute Free Energy Differences Between Molecular Mechanical and Quantum Mechanical Representations of Molecular Systems. *J. Phys. Chem. Lett.* **2015**, 6, 4850-4856.
46. Procacci, P.; Marsili, S., Energy dissipation asymmetry in the non equilibrium folding/unfolding of the single molecule alanine decapeptide. *Chemical Physics* **2010**, 375, 8-15.
47. Wang, X.; Xingzhao, T.; Boming, D.; John Z. H., Z.; Sun, Z., BAR-based Optimum Adaptive Steered MD for Configurational Sampling. *J. Comput. Chem.* **2019**, 40, 1270-1289.
48. Procacci, P., Methodological uncertainties in drug-receptor binding free energy predictions based on classical molecular dynamics. *Curr. Opin. Struct. Biol.* **2021**, 67, 127-134.

49. Swope, W. C., A computer simulation method for the calculation of equilibrium constants for the formation of physical clusters of molecules: Application to small water clusters. *J. Chem. Phys.* **1982**, 76, 637.
50. Pham, T. T.; Shirts, M. R., Identifying low variance pathways for free energy calculations of molecular transformations in solution phase. *J. Chem. Phys.* **2011**, 135, 034114.
51. Procacci, P.; Chelli, R., Statistical Mechanics of Ligand–Receptor Noncovalent Association, Revisited: Binding Site and Standard State Volumes in Modern Alchemical Theories. *J. Chem. Theory Comput.* **2017**, 13, 1924-1933.
52. Wang, X.; Tu, X.; Zhang, J. Z. H.; Sun, Z., BAR-based Optimum Adaptive Sampling Regime for Variance Minimization in Alchemical Transformation: The Nonequilibrium Stratification. *Phys. Chem. Chem. Phys.* **2018**, 20, 2009-2021.
53. Shirts, M. R.; Pande, V. S., Solvation free energies of amino acid side chain analogs for common molecular mechanics water models. *J. Chem. Phys.* **2005**, 122, 134508.
54. Hummer, G.; Pratt, L. R.; Garcia, A. E., Hydration free energy of water. *Journal of Physical Chemistry* **1995**, 99, 14188-14194.
55. Sun, Z. X.; Wang, X. H.; Zhang, J. Z. H., BAR-based Optimum Adaptive Sampling Regime for Variance Minimization in Alchemical Transformation. *Phys. Chem. Chem. Phys.* **2017**, 19, 15005-15020.
56. Huai, Z.; Sun, Z., Titration of Adenine in a GA mismatch with Grand Canonical Simulations. *Journal of Computational Biophysics and Chemistry* **2020**, 1-9.
57. Bruckner, S.; Boresch, S., Efficiency of alchemical free energy simulations. II. Improvements for thermodynamic integration. *J. Comput. Chem.* **2011**, 32, 1320–1333.
58. Resat, H.; Mezei, M., Studies on free energy calculations. I. Thermodynamic integration using a polynomial path. *J. Chem. Phys.* **1993**, 99, 6052-6061.
59. Resat, H.; Mezei, M., Studies on free energy calculations. II. A theoretical approach to molecular solvation. *J. Chem. Phys.* **1994**, 101, 6126-6140.
60. Paliwal, H.; Shirts, M. R., A Benchmark Test Set for Alchemical Free Energy Transformations and Its Use to Quantify Error in Common Free Energy Methods. *J. Chem. Theory Comput.* **2011**, 7, 4115-34.
61. Fenwick, M. K.; Escobedo, F. A., On the use of Bennett's acceptance ratio method in multi-canonical-type simulations. *J. Chem. Phys.* **2004**, 120, 3066-74.
62. Sun, Z.; Wang, X.; Zhang, J. Z., Determination of Binding Affinities of 3-Hydroxy-3-Methylglutaryl Coenzyme A Reductase Inhibitors from Free Energy calculation. *Chemical Physics Letters* **2019**, 723, 1-10.
63. Huai, Z.; Yang, H.; Li, X.; Sun, Z., SAMPL7 TrimerTrip host-guest binding affinities from extensive alchemical and end-point free energy calculations. *Journal of Computer-Aided Molecular Design* **2020**.
64. Sun, Z.; Wang, X.; Zhang, J. Z., Theoretical understanding of the thermodynamics and interactions in transcriptional regulator TtgR-ligand binding. *Phys. Chem. Chem. Phys.* **2020**, 22, 1511-1524.
65. Sun, Z.; Wang, X.; Zhao, Q.; Zhu, T., Understanding Aldose Reductase-Inhibitors interactions with free energy simulation. *Journal of Molecular Graphics and Modelling* **2019**, 91, 10-21.
66. Wang, X.; Sun, Z., Understanding PIM-1 kinase inhibitor interactions with free energy simulation. *Phys. Chem. Chem. Phys.* **2019**, 21, 7544-7558.
67. Heimdal, J.; Rydberg, P.; Ryde, U., Protonation of the proximal histidine ligand in heme peroxidases. *J. Phys. Chem. B* **2008**, 112, 2501-10.
68. Mikulskis, P.; Cioloboc, D.; Andrejić, M.; Khare, S.; Brorsson, J.; Genheden, S.; Mata, R. A.; Söderhjelm, P.; Ryde, U., Free-energy perturbation and quantum mechanical study of SAMPL4 octa-acid host-guest binding energies. *Journal of computer-aided molecular design* **2014**, 28, 375-400.
69. Fox, S. J.; Pittock, C.; Tautermann, C. S.; Fox, T.; Christ, C.; Malcolm, N. O.; Essex, J. W.; Skylaris, C. K., Free energies of binding from large-scale first-principles quantum mechanical calculations: application to ligand hydration energies. *J. Phys. Chem. B* **2013**, 117, 9478-85.
70. Genheden, S.; Ryde, U.; Söderhjelm, P., Binding affinities by alchemical perturbation using QM/MM with a large QM system and polarizable MM model. *J. Comput. Chem.* **2015**, 2114-2124.
71. Genheden, S.; Martinez, A. I. C.; Criddle, M. P.; Essex, J. W., Extensive all-atom Monte Carlo sampling and QM/MM corrections in the SAMPL4 hydration free energy challenge. *Journal of Computer-Aided Molecular Design* **2014**, 28, 187-200.

72. Fox, S. J.; Pittock, C.; Tautermann, C. S.; Fox, T.; Christ, C.; Malcolm, N. O. J.; Essex, J. W.; Skylaris, C. K., Free Energies of Binding from Large-Scale First-Principles Quantum Mechanical Calculations: Application to Ligand Hydration Energies. *J. Phys. Chem. B* **2013**, 117, 9478-85.

73. Woods, C. J.; Manby, F. R.; Mulholland, A. J., An efficient method for the calculation of quantum mechanics/molecular mechanics free energies. *J. Chem. Phys.* **2008**, 128, 152-159.

74. Caveayland, C.; Skylaris, C. K.; Essex, J. W., Direct Validation of the Single Step Classical to Quantum Free Energy Perturbation. *J. Phys. Chem. B* **2014**, 119, 1017-25.

75. Rod, T. H.; Ryde, U., Quantum mechanical free energy barrier for an enzymatic reaction. *Phys. Rev. Lett.* **2005**, 94.

76. Lameira, J. S.; Kupchencko, I.; Warshel, A., Enhancing Paradynamics for QM/MM Sampling of Enzymatic Reactions. *J. Phys. Chem. B* **2016**, 120, 2155.

77. Klimovich, P. V.; Shirts, M. R.; Mobley, D. L., Guidelines for the Analysis of Free Energy Calculations. *Journal of Computer-Aided Molecular Design* **2015**, 29, 397-411.

78. Wang, X.; He, Q.; Sun, Z., BAR-Based Multi-Dimensional Nonequilibrium Pulling for Indirect Construction of a QM/MM Free Energy Landscape. *Phys. Chem. Chem. Phys.* **2019**, 21, 6672-6688

79. Procacci, P.; Guarnieri, G., SAMPL7 blind predictions using nonequilibrium alchemical approaches. *Journal of Computer-Aided Molecular Design* **2021**.

80. Sun, Z., SAMPL7 TrimerTrip Host-Guest Binding Poses and Binding Affinities from Spherical-Coordinates-Biased Simulations. *Journal of Computer-Aided Molecular Design* **2020**.

81. Gao, J.; Luque, F. J.; Orozco, M., Induced dipole moment and atomic charges based on average electrostatic potentials in aqueous solution. *J. Chem. Phys.* **1993**, 98, 2975-2982.

82. Luzhkov, V.; Warshel, A., Microscopic models for quantum mechanical calculations of chemical processes in solutions: LD/AMPAC and SCAAS/AMPAC calculations of solvation energies. *J. Comput. Chem.* **1992**, 13, 199–213.

83. Wesolowski, T.; Warshel, A., Ab Initio Free Energy Perturbation Calculations of Solvation Free Energy Using the Frozen Density Functional Approach. *Journal of Physical Chemistry* **1994**, 98, 5183-5187.

84. Gao, J.; Xia, X., A priori evaluation of aqueous polarization effects through Monte Carlo QM-MM simulations. *Science* **1992**, 258, 631-5.

85. Zheng, Y. J.; Merz, K. M., Mechanism of the human carbonic anhydrase II-catalyzed hydration of carbon dioxide. *Journal of the American Chemical Society* **1992**, 114, 10498-10507.

86. Plotnikov, N. V.; Warshel, A., Exploring, refining, and validating the paradynamics QM/MM sampling. *J. Phys. Chem. B* **2012**, 116, 10342-10356.

87. Bentzien, J.; Muller, R. P.; Florián, J.; Warshel, A., Hybrid ab initio quantum mechanics/molecular mechanics calculations of free energy surfaces for enzymatic reactions: the nucleophilic attack in subtilisin. *J. Phys. Chem. B* **1998**, 102, 2293-2301.

88. Plotnikov, N.; Kamerlin, S. C. L.; Warshel, A., ParaDynamics: An Effective and Reliable Model for Ab Initio QM/MM Free Energy Calculations and Related Tasks. *J. Phys. Chem. B* **2011**, 115, 7950-62.

89. Polyak, I.; Benighaus, T.; Boulanger, E.; Thiel, W., Quantum mechanics/molecular mechanics dual Hamiltonian free energy perturbation. *J. Chem. Phys.* **2013**, 139, 578.

90. Sun, Z.; Zhu, T.; Wang, X.; Mei, Y.; Zhang, J. Z., Optimization of convergence criteria for fragmentation methods. *Chemical Physics Letters* **2017**, 687, 163-170.

91. Liu, W.; Sakane, S.; And, R. H. W.; Doren, D. J., The Hydration Free Energy of Aqueous Na+ and Cl- at High Temperatures Predicted by ab Initio/Classical Free Energy Perturbation: 973 K with 0.535 g/cm3 and 573 K with 0.725 g/cm3. *J. Phys. Chem. A* **2002**, 106, 1409-1418.

92. Olsson, M. A.; Söderhjelm, P.; Ryde, U., Converging ligand-binding free energies obtained with free-energy perturbations at the quantum mechanical level. *J. Comput. Chem.* **2016**, 37, 1589-1600.

93. Zhaoxi, S.; Zhirong, L., *BAR-based Multi-dimensional Nonequilibrium Pulling for Indirect Construction of QM/MM Free Energy Landscapes: Varying the QM Region*. 2021.

94. Hummer, G.; Szabo, A., From the Cover: Free energy reconstruction from nonequilibrium single-molecule pulling experiments. *Proceedings of the National Academy of Science* **2001**, 98, 3658-3661.

95. Hummer, G.; Szabo, A., Free Energy Reconstruction from Nonequilibrium Single-molecule Pulling Experiments. *Proc. Natl. Acad. Sci. USA* **2001**, 98, 3658-3661.
96. Hummer, G.; Szabo, A., Free Energy Surfaces from Single-molecule Force Spectroscopy. *Cheminform* **2005**, 36, 504-513.
97. Paramore, S.; Ayton, G. S.; Voth, G. A., Extending the Fluctuation Theorem to Describe Reaction Coordinates. *J. Chem. Phys.* **2007**, 126, 051102.
98. Balsera; Stepaniants; Izrailev; Oono; Schulten, Reconstructing potential energy functions from simulated force-induced unbinding processes. *Biophysical Journal* **1997**, 73, 1281.
99. Marsili, S.; Procacci, P., Free energy reconstruction in bidirectional force spectroscopy experiments: The effect of the device stiffness. *J. Phys. Chem. B* **2010**, 114, 2509-2516.
100. Jarzynski, C., Equilibrium free-energy differences from nonequilibrium measurements: A master-equation approach. *Phys. Rev. E* **1997**, 56, 5018-5035.
101. Kirkwood, J. G., Statistical Mechanics of Fluid Mixtures. *J. Chem. Phys.* **1935**, 3, 300.
102. Pearlman, D. A.; Kollman, P. A., The lag between the Hamiltonian and the system configuration in free energy perturbation calculations. *Journal of Chemical Physics* **1989**, 91, 7831-7839.
103. Straatsma, T. P.; Mccammon, J. A., Treatment of rotational isomers in free energy calculations. II. Molecular dynamics simulation study of 18-crown-6 in aqueous solution as an example of systems with large numbers of rotational isomeric states. *J. Chem. Phys.* **1989**, 91, 3631-3637.
104. Rodriguez, A.; Tsallis, C., A generalization of the cumulant expansion. Application to a scale-invariant probabilistic model. *Journal of mathematical physics* **2010**, 51, 073301.
105. Hummer, G., Fast-growth thermodynamic integration: Error and efficiency analysis. *J. Chem. Phys.* **2001**, 114, 7330-7337.
106. Kubo, R., Generalized cumulant expansion method. *Journal of the Physical Society of Japan* **1962**, 17, 1100-1120.
107. Huai, Z.; Shen, Z.; Sun, Z., Binding Thermodynamics and Interaction Patterns of Inhibitor-Major Urinary Protein-I Binding from Extensive Free-Energy Calculations: Benchmarking AMBER Force Fields. *J. Chem. Inf. Model.* **2021**, 61, 284-297.
108. Sun, Z.; Wang, X.; Song, J., Extensive Assessment of Various Computational Methods for Aspartate's pKa Shift. *J. Chem. Inf. Model.* **2017**, 57, 1621-1639.
109. Ozer, G.; Valeev, E. F.; Quirk, S.; Hernandez, R., Adaptive Steered Molecular Dynamics of the Long-Distance Unfolding of Neuropeptide Y. *J. Chem. Theory Comput.* **2010**, 6, 3026-3038.
110. Ozer, G.; Quirk, S.; Hernandez, R., Adaptive steered molecular dynamics: Validation of the selection criterion and benchmarking energetics in vacuum. *J. Chem. Phys.* **2012**, 136, 215104.
111. Ozer, G.; Quirk, S.; Hernandez, R., Thermodynamics of Decaalanine Stretching in Water Obtained by Adaptive Steered Molecular Dynamics Simulations. *J. Chem. Theory Comput.* **2012**, 8, 4837-4844.
112. Soares, C. M.; Bureau, H. R.; Merz, D. R.; Hershkovits, E.; Quirk, S.; Hernandez, R., Constrained Unfolding of a Helical Peptide: Implicit versus Explicit Solvents. *Plos One* **2015**, 10, e0127034.
113. Ozer, G.; Keyes, T.; Quirk, S.; Hernandez, R., Multiple branched adaptive steered molecular dynamics. *J. Chem. Phys.* **2014**, 141, 064101.
114. Dewar, M. J. S.; Zoebisch, E. G.; Healy, E. F.; Stewart, J. J. P., Development and use of quantum mechanical molecular models. 76. AM1: a new general purpose quantum mechanical molecular model. *Journal of the American Chemical Society* **1985**, 107, 3902-3909.
115. Stewart, J. J., Optimization of parameters for semiempirical methods V: modification of NDDO approximations and application to 70 elements. *Journal of Molecular modeling* **2007**, 13, 1173-1213.
116. Dewar, M. J. S.; Thiel, W., Ground states of molecules. 38. The MNDO method. Approximations and parameters. *Journal of the American Chemical Society* **1977**, 99, 4899-4907.
117. Roothaan, C. C. J., New Developments in Molecular Orbital Theory. *Rev. Mod. Phys.* **1951**, 23, 69-89.
118. Pople, J. A.; Nesbet, R. K., Self‐Consistent Orbitals for Radicals. *J. Chem. Phys.* **1954**, 22, 571-572.
119. Mcweeny, R.; Diercksen, G., Self‐Consistent Perturbation Theory. II. Extension to Open Shells. *J. Chem. Phys.* **1968**, 49, 4852-4856.
120. Head-Gordon, M.; Head-Gordon, T., Analytic MP2 frequencies without fifth-order storage. Theory and application to

bifurcated hydrogen bonds in the water hexamer. *Chemical Physics Letters* **1994**, 220, 122-128.
121. Frisch, M. J.; Head-Gordon, M.; Pople, J. A., A direct MP2 gradient method. *Chemical Physics Letters* **1990**, 166, 275-280.
122. Head-Gordon, M.; Pople, J. A.; Frisch, M. J., MP2 energy evaluation by direct methods. *Chemical Physics Letters* **1988**, 153, 503-506.
123. Frisch, M. J.; Head-Gordon, M.; Pople, J. A., Semi-direct algorithms for the MP2 energy and gradient. *Chemical physics letters* **1990**, 166, 281-289.
124. Stephens, P. J.; Devlin, F. J.; Chabalowski, C. F.; Frisch, M. J., Ab Initio Calculation of Vibrational Absorption and Circular Dichroism Spectra Using Density Functional Force Fields. *Journal of Physical Chemistry* **1994**, 98, 11623-11627.
125. Becke, A. D., Density‐functional thermochemistry. IV. A new dynamical correlation functional and implications for exact‐exchange mixing. *J. Chem. Phys.* **1996**, 104, 1040-1046.
126. Hertwig, R. H.; Koch, W., On the parameterization of the local correlation functional. What is Becke-3-LYP? *Chemical Physics Letters* **1997**, 268, 345-351.
127. Chai, J. D.; Head-Gordon, M., Systematic Optimization of Long-Range Corrected Hybrid Density Functionals. *J. Chem. Phys.* **2008**, 128, 57-63.
128. Rocha, G. B.; Freire, R. O.; Simas, A. M.; Stewart, J. J. P., RM1: A reparameterization of AM1 for H, C, N, O, P, S, F, Cl, Br, and I. *J. Comput. Chem.* **2006**, 27, 1101-1111.
129. Maier, J. A.; Martinez, C.; Kasavajhala, K.; Wickstrom, L.; Hauser, K. E.; Simmerling, C., ff14SB: Improving the Accuracy of Protein Side Chain and Backbone Parameters from ff99SB. *J. Chem. Theory Comput.* **2015**, 11, 3696-3713.
130. Pastor, R. W.; Brooks, B. R.; Szabo, A., An analysis of the accuracy of Langevin and molecular dynamics algorithms. *Mol. Phys.* **1988**, 65, 1409-1419.
131. Case, D. A.; Cheatham, T. E.; Tom, D.; Holger, G.; Luo, R.; Merz, K. M.; Alexey, O.; Carlos, S.; Bing, W.; Woods, R. J., The Amber Biomolecular Simulation Programs. *J. Comput. Chem.* **2005**, 26, 1668-1688.
132. Frisch, M.; Trucks, G.; Schlegel, H.; Scuseria, G.; Robb, M.; Cheeseman, J.; Scalmani, G.; Barone, V.; Mennucci, B.; Petersson, G., GAUSSIAN09, Gaussian, Inc., Wallingford, CT, USA,(2009). *Google Scholar* **2016**.

Table 1. Mean absolute error of the indirect RM1 estimates in kcal/mol. 8 different initial configurations are tested to initiate the multi-dimensional ASMD pulling. The pulling speed in the configurational space is 10 ps per 3º segment. Two pulling speeds including a change of 0.1 per time step and 0.01 per time step are tested in the alchemical space. The errors for the averaged indirect estimates over the last 5 initial configurations are also shown. We can see that the systematic errors of the indirect estimates are reduced upon increased pulling time in the alchemical space. The averaged results are significantly improved over independent trails.

Hamiltonians / Trail	0.1 to RM1		0.01 to RM1	
	AM1	MNDO	AM1	MNDO
1	0.44	0.28	0.23	0.07
2	0.37	0.43	0.13	0.15
3	0.43	0.41	0.13	0.13
4	0.37	0.70	0.11	0.14
5	0.27	0.22	0.23	0.12
6	0.79	1.13	-	-
7	0.35	0.37	-	-
8	0.21	0.34	-	-
average over 5 trails	0.11	0.30	0.08	0.10

Table 2. Efficiency comparison of direct and indirect free energy simulations under the HF Hamiltonian. The calculation of the computational cost is similar to the case of our previous BAR-based method. There are N_{segments} segments in stratified pulling and the number of realizations in each segment is N_{traj}. The total simulation time in the direct scheme is given by $N_{\text{segments}} * N_{\text{traj}} * (\phi_{\text{NEW}} + \phi_{\text{eq}})$, while the total simulation time in the indirect scheme is the sum of $N_{\text{segments,SQM}} * N_{\text{traj.SQM}} * (\phi_{\text{NEW,SQM}} + \phi_{\text{eq,SQM}})$ at SQM level and $N_{\text{traj,SQM->QM}} * (\phi_{\text{NEW,SQM->QM}} + \phi_{\text{eq,SQM}})$ in the SQM-to-QM correction. As the selection criterion eliminates the equilibrium sampling for initial configurations, ϕ_{eq} becomes 0. The simulation time at QM level is scaled by the ratio of computational cost under QM Hamiltonian and that under SQM Hamiltonian in Table S1 to provide the effective simulation time at SQM level, enabling the direct comparison between computational costs of different levels of theory. Note that the sample size for the correction term is the sum of 5 repeats of the 10-step SQM-to-QM transformation, corresponding to the sample size of 25 for the SQM->HF perturbation. If the pulling time of 100 steps is used for the alchemical transformation, the speedup of the indirect method would be about 200 folds.

Terms / Simulation	ϕ_{eq} for each initial configuration (ps)	ϕ_{NEW} in each segment (ps)	Number of segments	Number of realizations per segment	Total simulation time (ps) scaled to SQM Hamiltonian	Relative efficiency
direct SQM	0	10	120	20	24000.00	3343.64
SQM->HF	0	0.005	120	25	50154.60	-
HF->SQM	-	-	-	-	0.00	-
indirect HF	-	-	-	-	74154.60	1082.16
direct HF	0	10	120	20	80247357.45	1.00

Table 3. Efficiency comparison of direct and indirect nonequilibrium free energy simulations with the current JI-based ASMD method and the previously proposed BAR-based method. The total simulation time in direct scheme is given by $N_{\text{segments}} * N_{\text{traj}} * (\phi_{\text{NEW}} + \phi_{\text{eq}})$, while the total simulation time in the indirect scheme is the sum of $N_{\text{segments,small}} * N_{\text{traj,small}} * (\phi_{\text{NEW,small}} + \phi_{\text{eq,small}})$ under the SQM Hamiltonian and $N_{\text{traj,small->large}} * (\phi_{\text{NEW,small->large}} + \phi_{\text{eq,small}}) + N_{\text{traj,large->small}} * (\phi_{\text{NEW,large->small}} + \phi_{\text{eq,large}})$ in the SQM-to-QM correction. N_{segments} is the number of segments and N_{traj} is the number of realizations per segment. The simulation time under the QM Hamiltonian is scaled by the ratio of computational cost QM/SQM in Table S1 to provide the effective simulation time at the SQM level, enabling the direct comparison between computational costs from methods. The statistics for the BAR-based method is borrowed from our previous work, Phys. Chem. Chem. Phys. 2019, 21, 21942-21959. As the BAR-based method is faster than ASMD in the construction of the free energy profiles in the configurational space, its computational cost of the direct free energy simulation (3.78 ns in the reference) is smaller than the ASMD one (24 ns). Therefore, the speedup of the multi-dimensional ASMD method is relatively modest compared with the ~1000-fold speedup shown in the previous table.

Terms / Simulation	ϕ_{eq} for each initial configuration (ps)	ϕ_{NEW} in each segment (ps)	Number of segments	Number of realizations per segment	Total simulation time (ps) scaled to SQM Hamiltonian	Relative efficiency
direct SQM	0	10	120	20	24000.00	526.62
SQM->HF	0	0.005	120	25	50154.60	-
HF->SQM	-	-	-	-	0.00	-
indirect HF	-	-	-	-	74154.60	170.44
direct HF	0.05	0.5x2=1	180	20	12638958.80	1.00

Fig. 1. a) An illustration of the Hamiltonian perturbation framework via EXP-based multi-dimensional nonequilibrium free energy calculations. The Hamiltonian perturbation is performed between neighboring states with nonequilibrium transformations. The Hamiltonian of the system at the k_1 th configurational state and k_2 th alchemical state is represented as H_{k_1,k_2}. The target free energy landscape is at the Hamiltonian state $K_2 = 2$. The indirect scheme performs direct free energy simulations at the Hamiltonian state $k_2 = 1$ to explore the configurational space, and adds the $H_{k_1,1}$-to-$H_{k_1,2}$ correction term to perturb the thermodynamic profile to the result at the target Hamiltonian state. The unidirectional arrows represent unidirectional pulling and unidirectional reweighting of the EXP or JI estimator. Only the transformations described with solid arrows are performed due to efficiency considerations in nonequilibrium free energy simulations. b) The thermodynamic cycle describing the dihedral flipping process with different descriptions of the ACE-NME system. The reaction coordinate is the backbone C-C-N-C dihedral. The free energy simulation exploring the configurational space is performed at some computationally efficient SQM levels, and the SQM-to-QM perturbation term is used to obtain the thermodynamic profiles at ab initio QM levels.

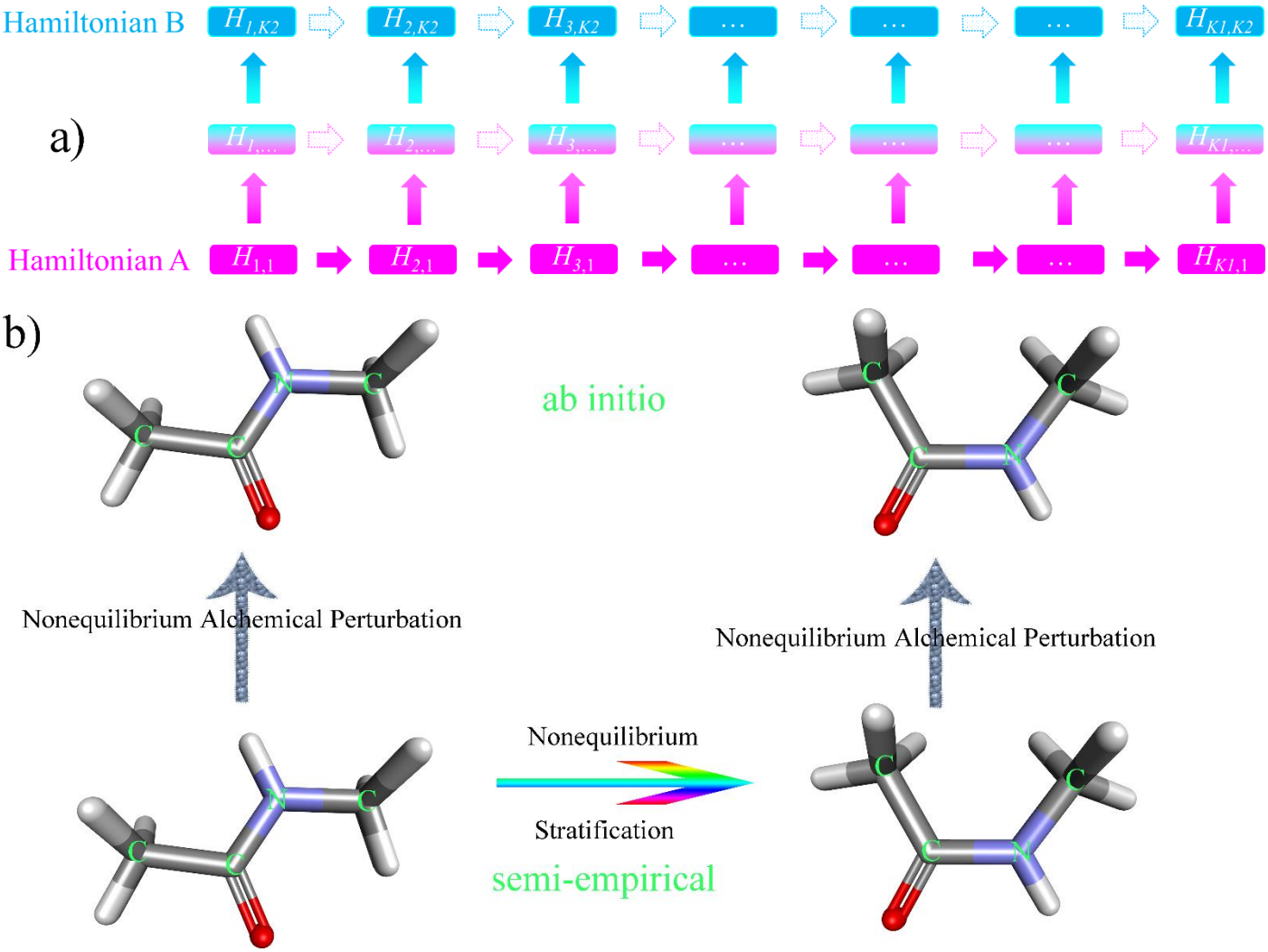

Fig. 2. a) The free energy profiles in the direct free energy simulation under the RM1 Hamiltonian with different pulling speeds. The number in the legend represents the number of MD steps for each nonequilibrium trajectory in each segment. As we are using 0.5 fs time steps, the pulling times of 10000 steps, 20000 steps and 30000 steps are equivalently 5 ps, 10 ps and 15 ps. We can see that the pulling speed of 10 ps per segment is sufficiently slow for converged estimates of the free energy profiles. b) The indirect estimates at the RM1 level with different sample sizes for the correction term in one seeding SMD trail. The alchemical order parameter is varied in 10 MD steps with a change of 0.1 per step. We can see that the 5-sample, 10-sample and 50-sample estimates with different estimators are virtually identical.

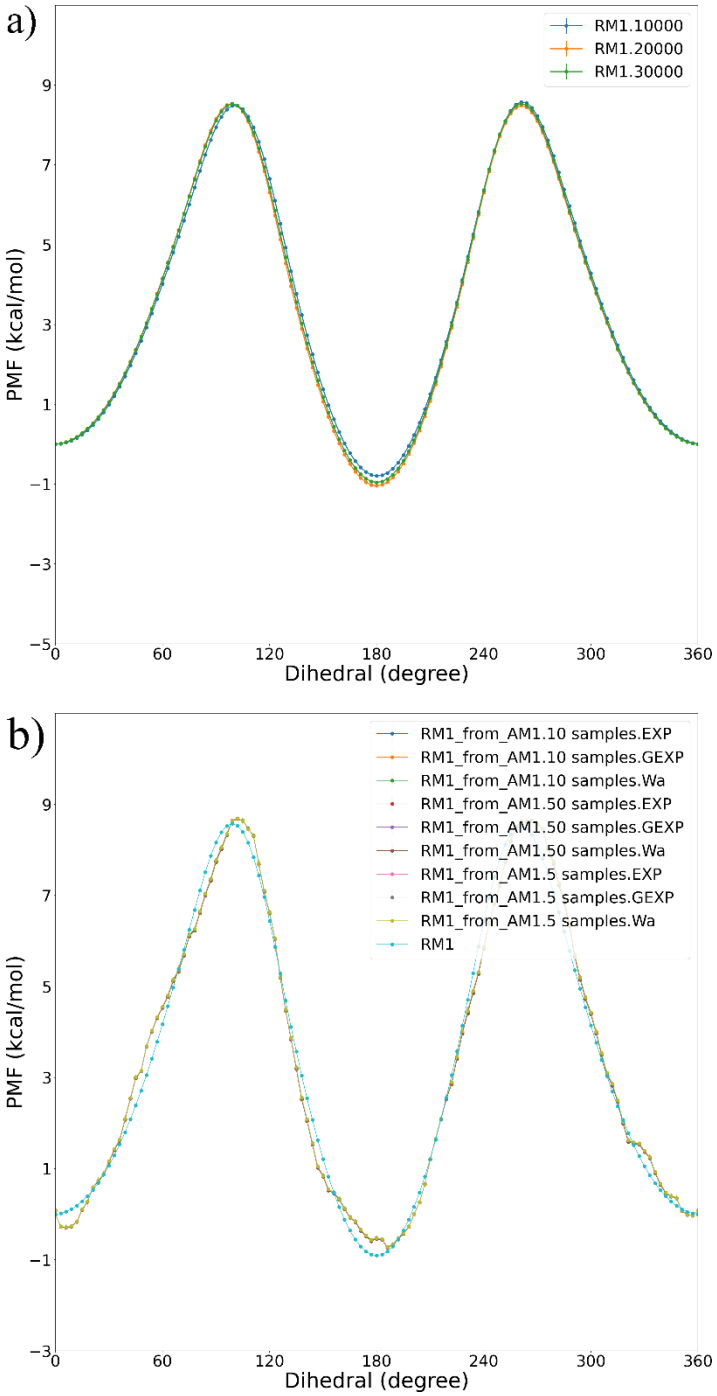

Fig. 3. The statistical uncertainty for the correction terms. a) The multi-dimensional SMD simulation is initiated from the 1st configuration with the pulling speed of 10 ps/segment. The AM1, MNDO and PM6 Hamiltonians are used to explore the configurational space, and the correction term is used to perturb the results to the RM1 level. As the differences between different SQM Hamiltonians and the target RM1 are different, the statistical errors for different SQM-to-RM1 corrections obtained from the same estimator are different. The statistical error of the GEXP estimator is extremely similar to that of the ordinary average Wa, due to the negligible dissipation or the width of the work distribution. As a result, the GEXP and the Wa estimates are virtually identical. b) The AM1-to-RM1 correction averaged over 5 initial configurations. The pulling speed of 0.1/step is used along the alchemical CV, while two pulling speeds of 10 ps/segment and 15 ps/segment are used along the configurational CV. We can see that the statistical error shows little dependence on the pulling speed in the configurational space.

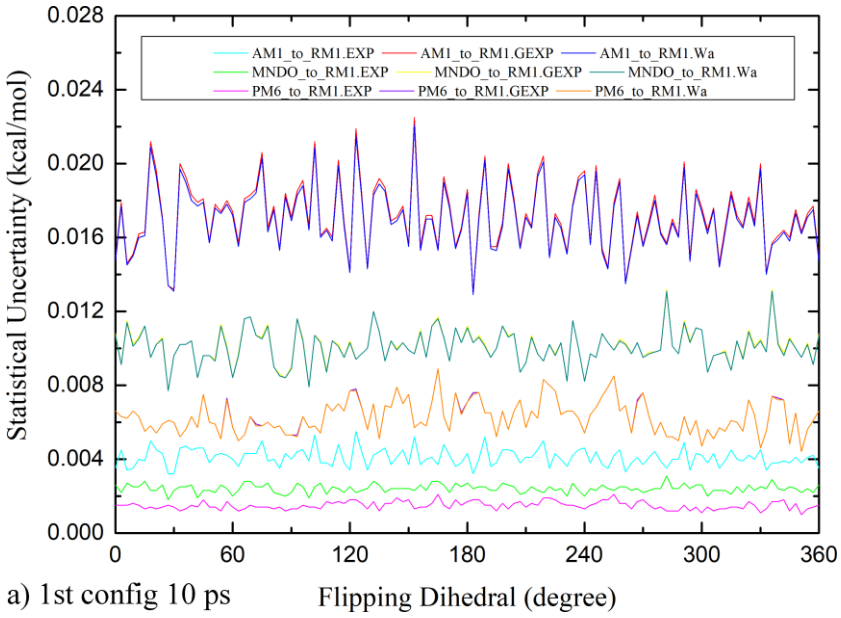

a) 1st config 10 ps

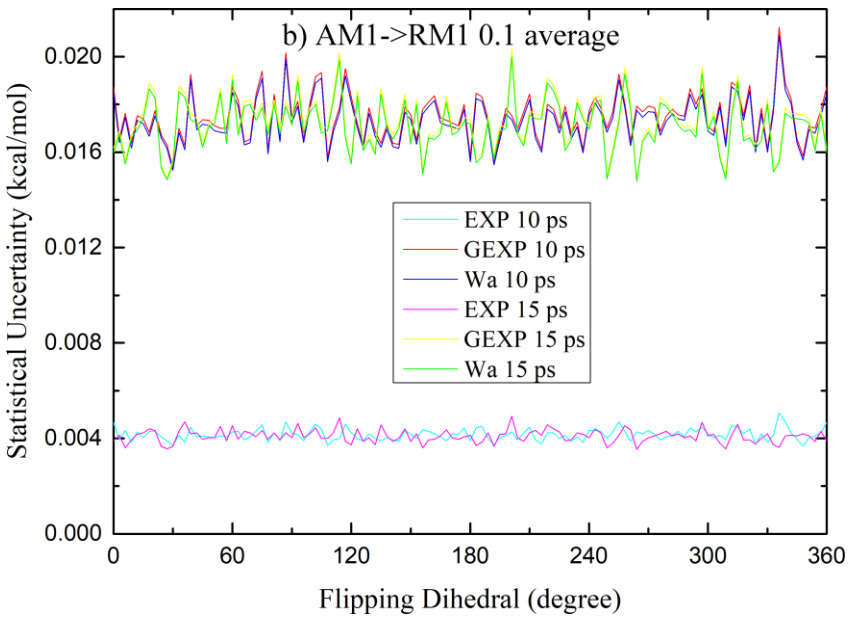

Fig. 4. Comparison between the direct and indirect results at the RM1 level with the pulling speed of 10 ps per 3º segment for nonequilibrium pulling in the configurational space. a) and c) are obtained from the same initial configuration to initiate the multi-dimensional ASMD simulation, while b) and d) are the averaged results over 5 initial configurations. For a) and b), the alchemical order parameter is varied in 10 MD steps with a change of 0.1 per step, while for c) and d), the alchemical CV is changed in 100 MD steps with a perturbation of 0.01 per time step. More detailed results for different initial configurations and pulling speeds are given in Fig. S2 and S3.

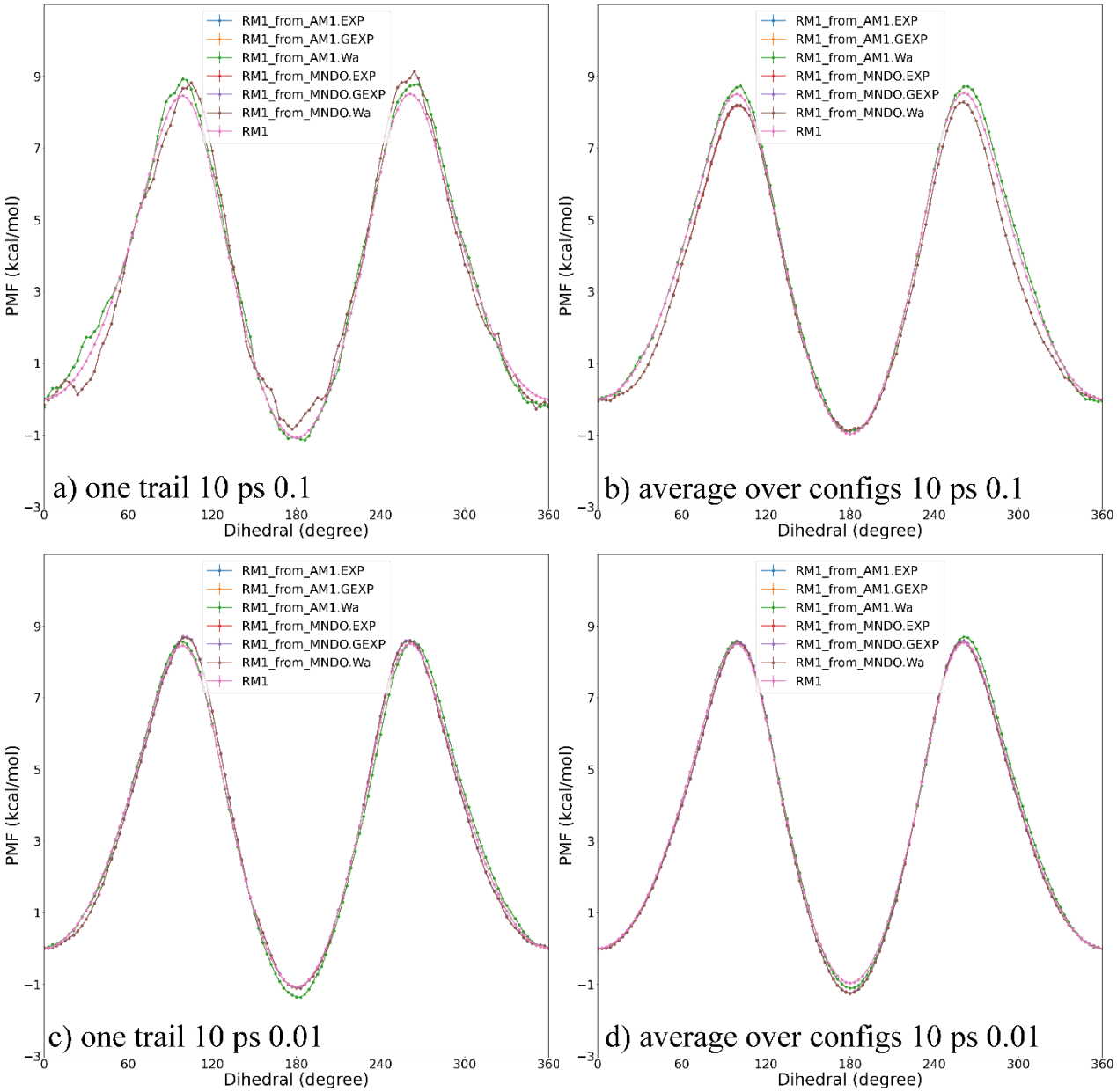

Supporting Information: Seeding the Multi-dimensional Nonequilibrium Pulling for Hamiltonian Variation: Indirect QM/MM Free Energy Simulations

Zhaoxi Sun[1*] and Qiaole He[2]

[1]*Beijing National Laboratory for Molecular Sciences, College of Chemistry and Molecular Engineering, Institute of Theoretical and Computational Chemistry, Peking University, Beijing 100871, China*

[2]*State Key Laboratory of Bioreactor Engineering, East China University of Science and Technology, 200237 Shanghai, China*

*To whom correspondence should be addressed: z.sun@pku.edu.cn

Table S1. The timing information (in ns/day) of SQM and QM calculations on a computing node with 384 GB memory and the CPU used is Intel(R) Xeon(R) Platinum 8160. A single core is used for this benchmark, which avoids the influence of parallelization-related issues. As the nonequilibrium trajectories are independent, the practical simulation speed is the same as these statistics. As the memory on each computing node is very large, no memory-related issue in QM calculations would influence the speed of calculation. The basis set of 6-31G* is employed in ab initio QM calculations. Different SQM simulations are of very similar computational costs, while the speed of ab initio QM calculations depends on the level of theory. Here, we only tested the HF Hamiltonian.

Hamiltonian / Terms	SQM	HF
speed(ns/day)	46.5	0.013907
speedup(SQM/QM)	1.00	3343.64

Table S2. Mean absolute error of the indirect estimates at ab initio QM levels in kcal/mol. 7 different initial configurations are tested to initiate the multi-dimensional ASMD pulling. The pulling speed in the configurational space is 10 ps per 3º segment. The alchemical perturbation is finished in 10 time steps with a change of 0.1 per step in the first 7 trails, while the last trail 0.01 uses 100 steps.

Hamiltonians / Trail	HF		
	AM1	MNDO	RM1
1	0.31	0.35	0.60
2	0.83	0.79	1.33
3	0.88	0.54	0.93
4	0.56	0.91	0.75
5	0.50	0.44	0.67
6	0.81	1.21	0.47
7	0.52	1.23	0.67
0.01	0.20	0.30	0.21

Fig. S1. Comparison between the direct and indirect estimates of the free energy profiles at the RM1 level initiated from different seeds (i.e., configurations) with different pulling speeds along the configurational CV or the alchemical CV. The configurational space is explored with the ASMD scheme with 20 samples in each stage at the PM6 level, and the RM1 result is obtained by the combination of the PM6 result and the PM6-to-RM1 unidirectional pulling. The pulling time 'x ps' denotes the pulling time for each segment along the configurational CV. The nonequilibrium transformation in the alchemical space is performed in 5 fs (i.e., 10 time steps with a change of 0.1 per step) for the first 5 subplots, while a smaller perturbation (0.01 per time step) and thus a longer pulling time is used for the last subplot. The exponential average EXP, the Gaussian approximation GEXP, and the ordinary average Wa are extremely similar, leading to overlaps of these curves in the plot. We can see that different initial configurations could lead to different systematic errors with a faster pulling speed along the alchemical CV, which could be eliminated when a slower pulling speed is employed.

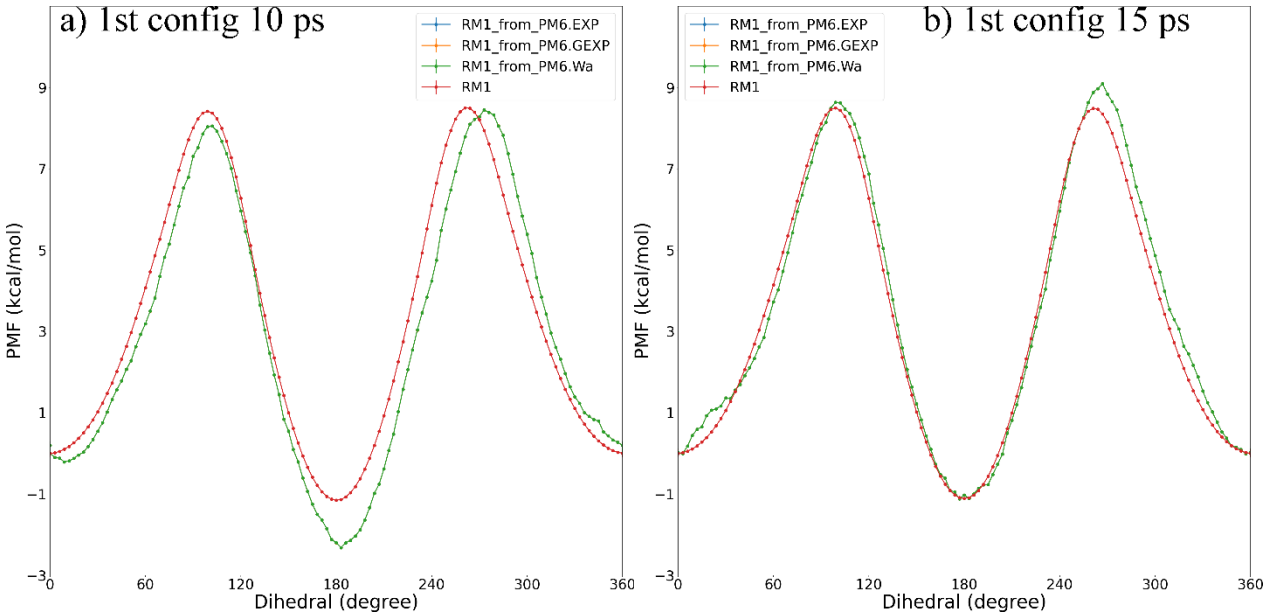

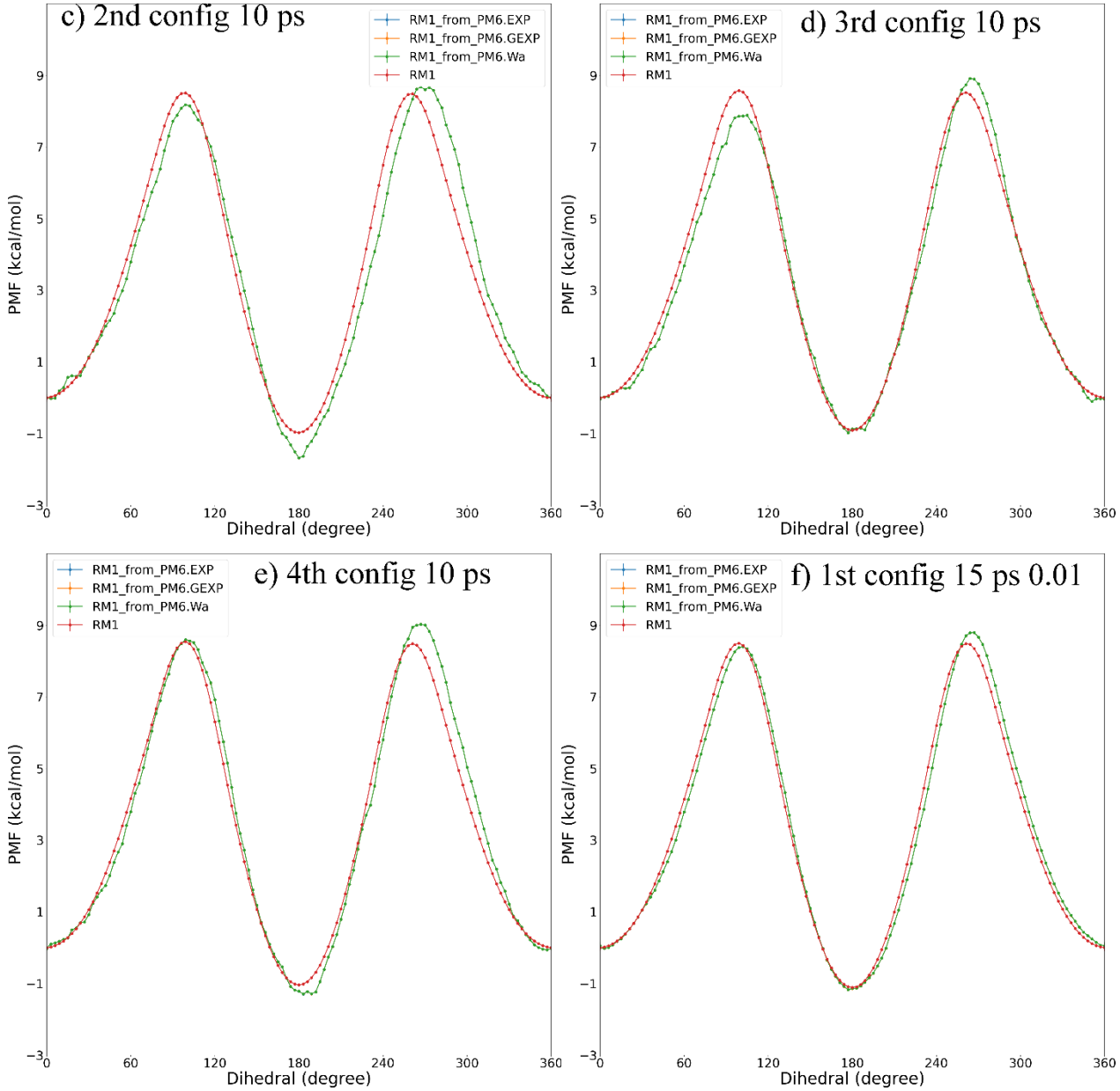
c) 2nd config 10 ps
d) 3rd config 10 ps
e) 4th config 10 ps
f) 1st config 15 ps 0.01
RM1_from_PM6.EXP
RM1_from_PM6.GEXP
RM1_from_PM6.Wa
RM1
PMF (kcal/mol)
Dihedral (degree)

Fig. S2. Comparison between the direct and indirect estimates of the free energy profiles at the RM1 level initiated from different seeds (i.e., configurations) with different pulling speeds along the configurational CV or the alchemical CV. The configurational space is explored with the ASMD scheme with 20 samples in each stage under the AM1 or MNDO Hamiltonians, and the RM1 result is obtained by the combination of the AM1 or MNDO result and the AM1-to-RM1 or MNDO-to-RM1 unidirectional pulling. The pulling time 'x ps' denotes the pulling time for each segment along the configurational CV. 8 different initial configurations are used for the seeding SMD simulations with the pulling speed of 10 ps per segment are used for the first 8 subplots a-h), while the first 3 configurations are used to initiate the seeding SMD simulations with a slower pulling speed of 15 ps per segment for the last 3 subplots i-k). The nonequilibrium transformation in the alchemical space is performed in 5 fs (i.e., 10 time steps with a change of 0.1 per step). The exponential average EXP, the Gaussian approximation GEXP, and the ordinary average Wa are extremely similar, leading to overlaps of these curves in the plot. Different initial configurations introduce different systematic errors, and averaging over these configurations could eliminate this systematic error, as shown in the main article. The pulling speeds of 10 ps/segment and 15 ps/segment along the configurational CV have little influence on the systematic error of the indirect results, as the latter is mainly introduced in the alchemical perturbation term.

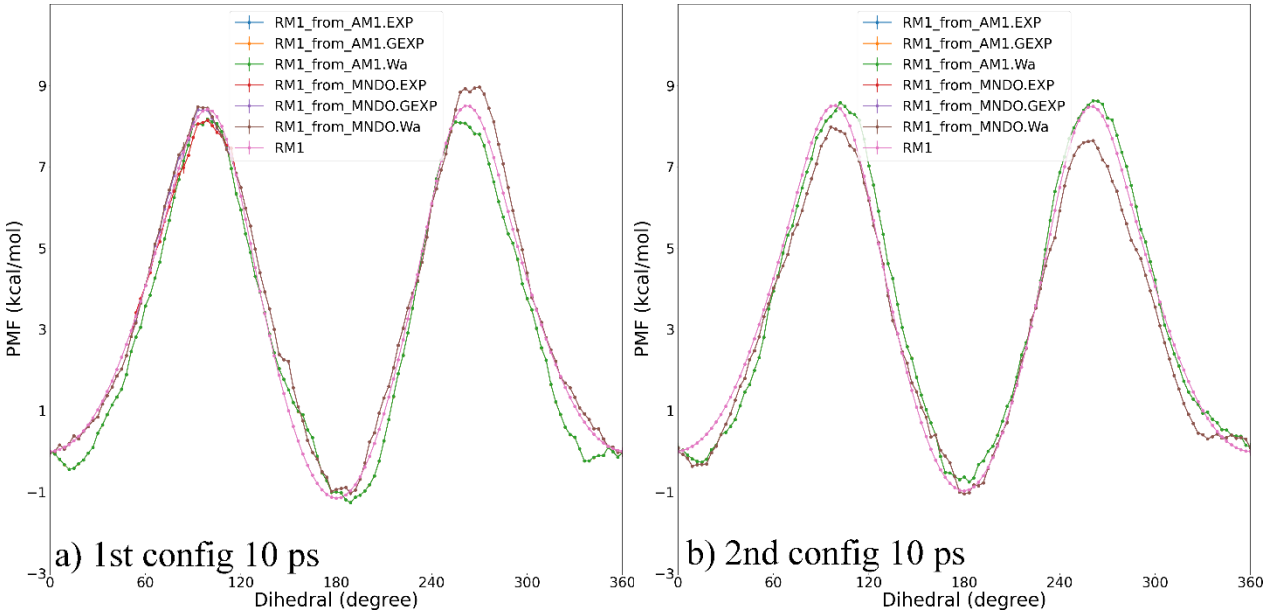

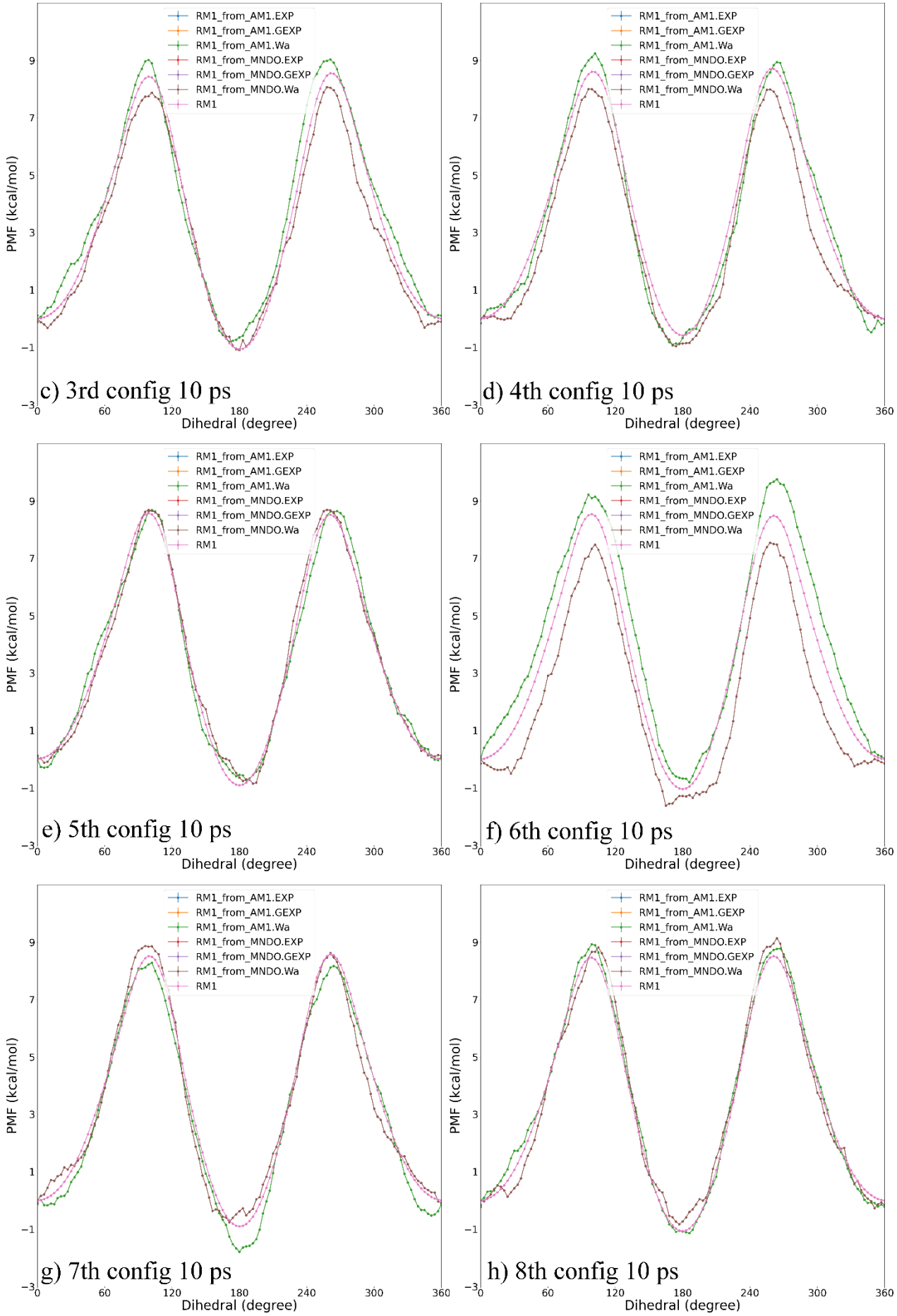
RM1_from_AM1.EXP
RM1_from_AM1.GEXP
RM1_from_AM1.Wa
RM1_from_MNDO.EXP
RM1_from_MNDO.GEXP
RM1_from_MNDO.Wa
RM1
PMF (kcal/mol)
Dihedral (degree)
c) 3rd config 10 ps
d) 4th config 10 ps
e) 5th config 10 ps
f) 6th config 10 ps
g) 7th config 10 ps
h) 8th config 10 ps

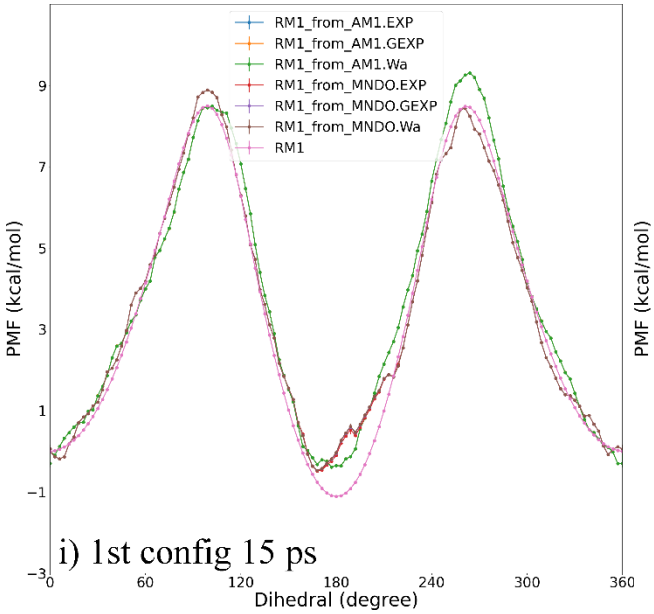
RM1_from_AM1.EXP
RM1_from_AM1.GEXP
RM1_from_AM1.Wa
RM1_from_MNDO.EXP
RM1_from_MNDO.GEXP
RM1_from_MNDO.Wa
RM1
PMF (kcal/mol)
Dihedral (degree)
i) 1st config 15 ps

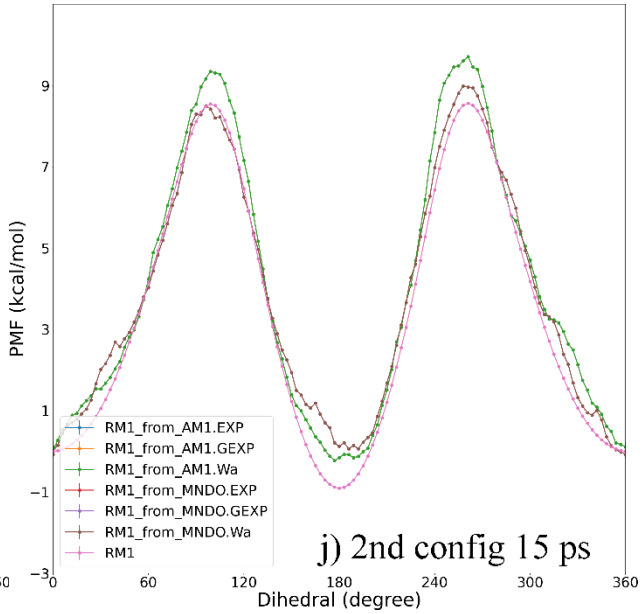
RM1_from_AM1.EXP
RM1_from_AM1.GEXP
RM1_from_AM1.Wa
RM1_from_MNDO.EXP
RM1_from_MNDO.GEXP
RM1_from_MNDO.Wa
RM1
PMF (kcal/mol)
Dihedral (degree)
j) 2nd config 15 ps

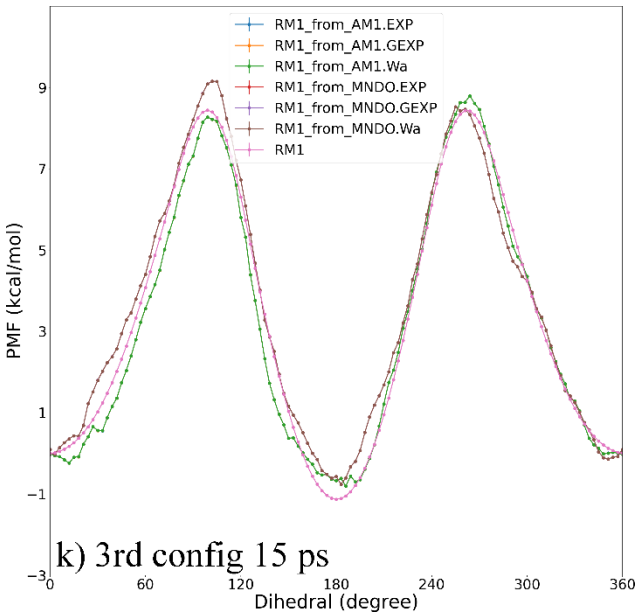
RM1_from_AM1.EXP
RM1_from_AM1.GEXP
RM1_from_AM1.Wa
RM1_from_MNDO.EXP
RM1_from_MNDO.GEXP
RM1_from_MNDO.Wa
RM1
PMF (kcal/mol)
Dihedral (degree)
k) 3rd config 15 ps

Fig. S3. Comparison between the direct and indirect estimates of the free energy profiles at the RM1 level initiated from different seeds (i.e., initial configurations) with different pulling speeds along the configurational CV or the alchemical CV. The configurational space is explored with the ASMD scheme with 20 samples in each stage under the AM1 or MNDO Hamiltonians, and the RM1 result is obtained by combining the AM1 or MNDO result and the AM1-to-RM1 or MNDO-to-RM1 unidirectional pulling. The pulling time 'x ps' denotes the pulling time for each segment along the configurational CV. Different initial configurations are used for the seeding SMD simulations with the pulling speed of 10 ps per segment are used for the first 4 subplots a-d), while the first 2 configurations are used to initiate the seeding SMD simulations with a slower pulling speed of 15 ps per segment for the last 2 subplots e-f). The nonequilibrium transformation in the alchemical space is performed in 50 fs (i.e., 100 time steps with a change of 0.01 per step). The exponential average EXP, the Gaussian approximation GEXP, and the ordinary average Wa are extremely similar, leading to overlaps of these curves in the plot. Compared with the indirect estimates obtained with a faster pulling speed along the alchemical CV shown in the previous figure, the current results are much closer to the direct free energy estimates, which indicates that the sampling in the nonequilibrium ensemble successfully eliminates the systematic bias introduced in the alchemical perturbation term. The pulling speed in the configurational space have little impact on the outcome.

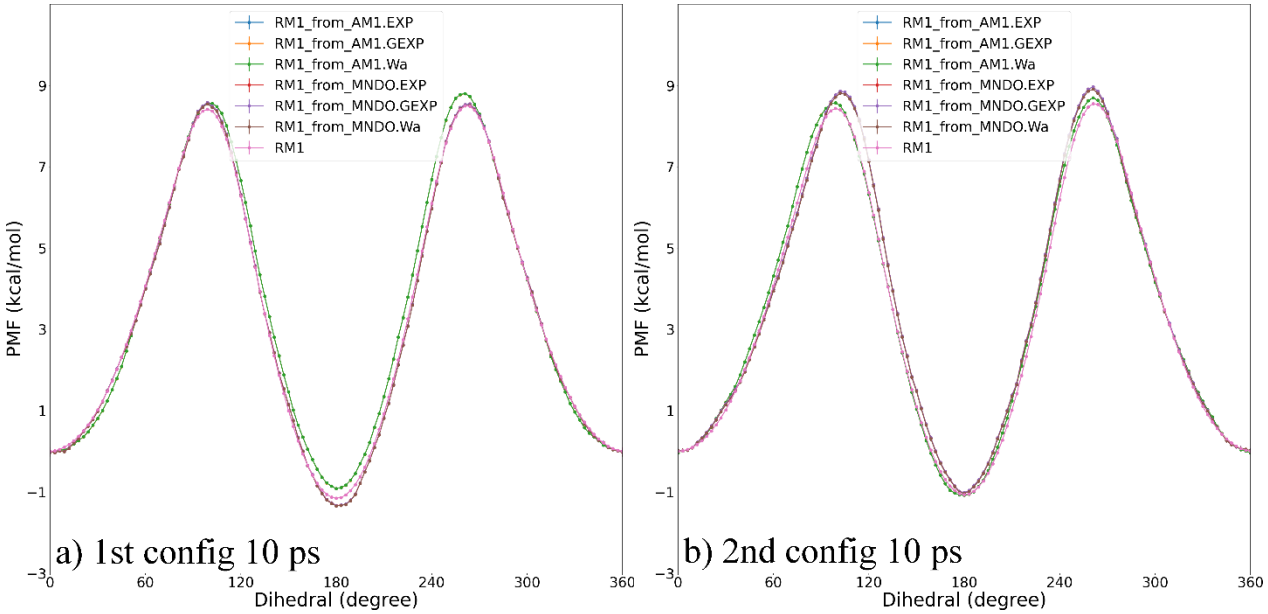

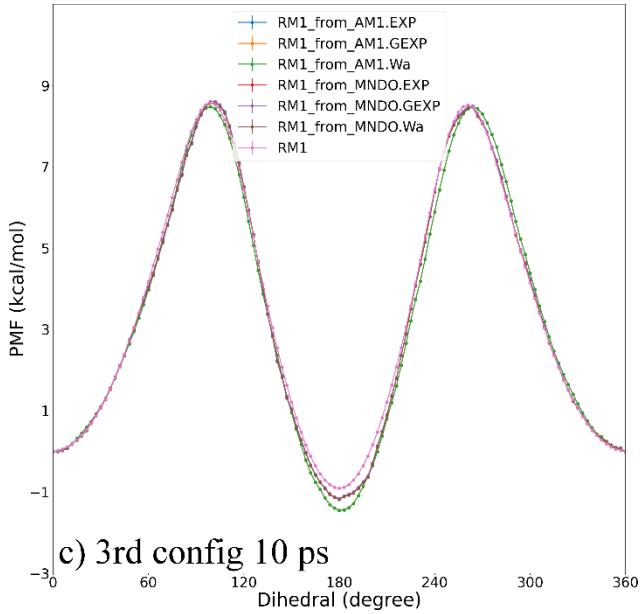
RM1_from_AM1.EXP
RM1_from_AM1.GEXP
RM1_from_AM1.Wa
RM1_from_MNDO.EXP
RM1_from_MNDO.GEXP
RM1_from_MNDO.Wa
RM1
PMF (kcal/mol)
Dihedral (degree)
c) 3rd config 10 ps

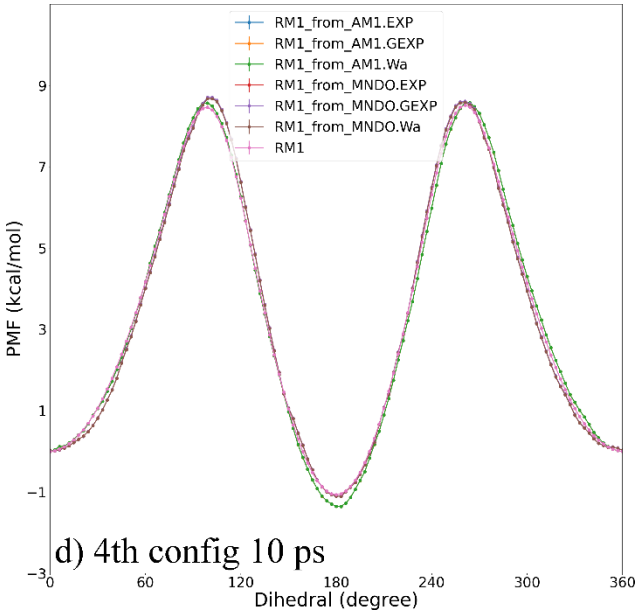
RM1_from_AM1.EXP
RM1_from_AM1.GEXP
RM1_from_AM1.Wa
RM1_from_MNDO.EXP
RM1_from_MNDO.GEXP
RM1_from_MNDO.Wa
RM1
PMF (kcal/mol)
Dihedral (degree)
d) 4th config 10 ps

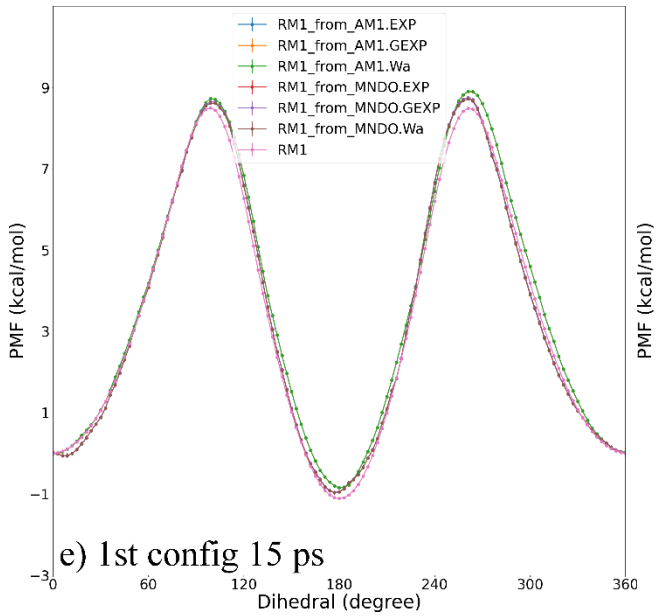
RM1_from_AM1.EXP
RM1_from_AM1.GEXP
RM1_from_AM1.Wa
RM1_from_MNDO.EXP
RM1_from_MNDO.GEXP
RM1_from_MNDO.Wa
RM1
PMF (kcal/mol)
Dihedral (degree)
e) 1st config 15 ps

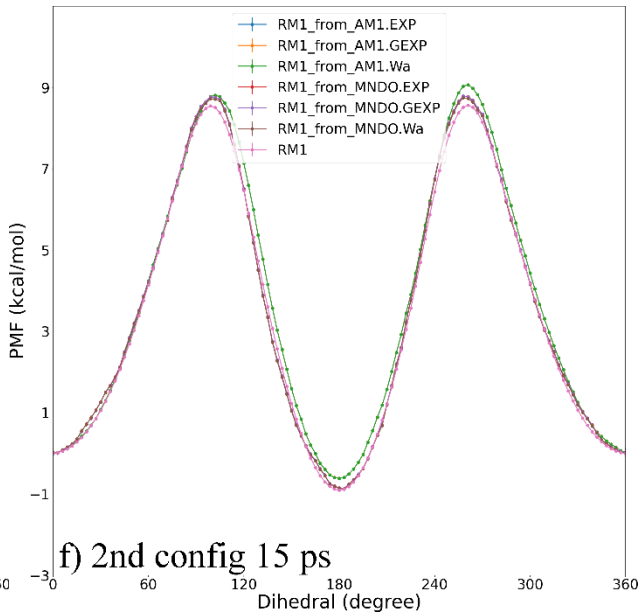
RM1_from_AM1.EXP
RM1_from_AM1.GEXP
RM1_from_AM1.Wa
RM1_from_MNDO.EXP
RM1_from_MNDO.GEXP
RM1_from_MNDO.Wa
RM1
PMF (kcal/mol)
Dihedral (degree)
f) 2nd config 15 ps